Sustainable Chemical Engineering
http://ojs.wiserpub.com/index.php/SCE/

Research Article

Computational Studies of Biodegradation of Polyester-Polyurethanes by Protease Enzyme

Baggya Karunarathna[1*], G. M. S. T. Gajasinghe[2], V. T. Hewage[2], K. K. Govender[3,4], M. B. A. Prashantha[2], J. D. Wanniarachchi[2]

[1]Department of Chemistry, Faculty of Science, Eastern University Sri Lanka, Chenkalady, Sri Lanka
[2]Department of Chemistry, Faculty of Applied Sciences, University of Sri Jayewardenepura, Sri Lanaka
[3]Department of Chemical Sciences, University of Johannesburg, P.O. Box 17011, Doornfontein Campus, 2028 Johannesburg, South Africa
[4]National Institute for Theoretical and Computational Sciences, NITheCS, Stellenbosch, South Africa
E-mail: baggyakarunarathna@gmail.com

Received: 24 June 2024; **Revised:** 15 August 2024; **Accepted:** 16 August 2024

Graphical Abstract

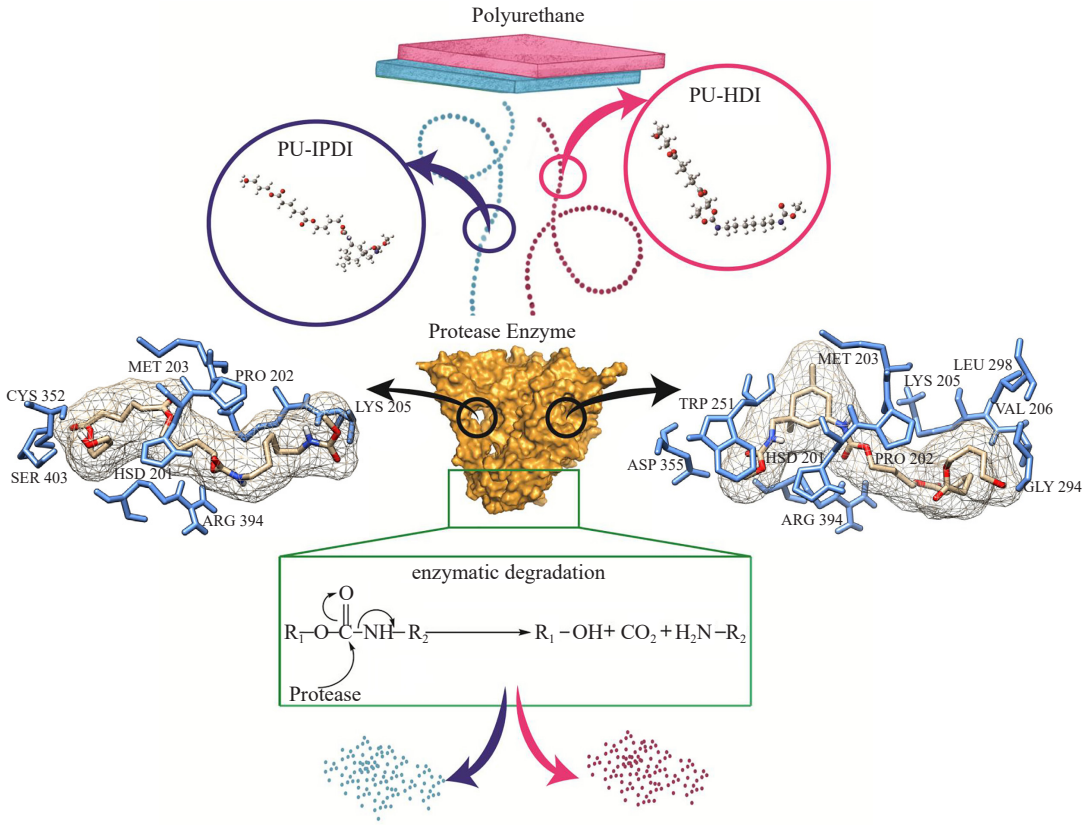

DOI: https://doi.org/10.37256/sce.5220245188

Abstract: Polyurethane (PU) is a widely used synthetic polymer with significant environmental concerns. Recent research into PU biodegradation, especially via protease enzymes, shows potential, yet the degradation mechanisms are not fully understood. This study investigates the binding interactions between protease and two PU variants: polybutylene adipate with 1,6-hexamethylene diisocyanate (PU-HDI) and 5-isocyanato-1-(isocyanatomethyl)-1,3,3-trimethylcyclohexane (PU-IPDI). Using 150 ns molecular dynamics (MD) simulations, a shift towards more stable conformations was observed, with residues in the most favored regions increasing from 63.2% to 86.3% in the Ramachandran plot. Density Functional Theory (DFT) optimized PU ligands were docked into the enzyme's binding pocket, and validated by tunnel analysis. Docking studies revealed distinct stabilizing interactions for each PU variant; PU-HDI's urethane linkage formed a strong hydrogen bond with HSD201, while PU-IPDI's urethane linkage bonded with ARG394 and PRO202. MD simulations confirmed the stability of these complexes, emphasizing persistent hydrogen bonds. Analysis of urethane bond lengths identified potential enzymatic degradation initiation sites. The binding of PU monomers reduced the protease enzyme's flexibility, indicating a significant structural impact. The MM/PBSA method confirmed substantial interactions between PU and the protease, supporting the study's findings. This research offers vital insights into aliphatic PU and protease interactions, advancing the development of biodegradable materials.

***Keywords*:** Polyurethane, HDI, IPDI, Bio degradations, DFT and MD simulations

1. Introduction

The steady growth of synthetic plastics and foams, with their greater strength-to-weight ratio, superior insulating properties, and energy absorption performance, has played a significant role in various industries and everyday life over the last few decades[1,2]. In 2018, PU emerged as one of the most dominant polymeric forms, boosting a global market value of 65.5 billion dollars[3]. Ranking 6th in the world for polymer manufacturing, the PU market is projected to witness substantial growth, reaching an estimated 105.2 billion dollars by the year 2025[3]. PU foams, in high demand, serve as crucial materials in the automobile industry. They find application in creating suspension insulators, bumpers, vehicle seats, headliners, and various other interior components. Beyond the automotive sector, these versatile foams are also extensively utilized in the furniture, insulation, healthcare, and home appliance industries[4-6].

Nevertheless, the benefits derived from PU are accompanied by the environmental challenge posed by their accumulation. With global plastic production projected to reach 311 million tons annually, a mere 14% of this vast quantity is collected for recycling. Consequently, the escalating volume of PU waste has evolved into a significant environmental concern[7,8]. In general, the waste management of PU involves various methods, including landfilling, physical and chemical recycling, and thermal degradation. These approaches are employed to address the environmental impact of PU waste and manage its disposal in a more sustainable manner[1,9]. Indeed, the methods employed for PU waste management come with significant challenges. Recycling, for instance, has the drawback that the material becomes unusable after a few cycles, limiting its effectiveness as a long-term solution. Additionally, incineration of plastics, including PU, has been observed to release toxic and greenhouse gases such as CO_2 and CO, along with heavy metals like cadmium and lead. These environmental concerns highlight the need for more sustainable and eco-friendly approaches to PU waste management[9-10]. Absolutely, biodegradation of plastics has garnered increased attention in recent years, thanks to its promising results and eco-friendly nature. Numerous publications are now focusing on the potential for microbial decomposition of plastic waste. This approach offers a more sustainable and environmentally friendly alternative to traditional disposal methods, as microorganisms break down the plastic into natural substances over time. Research in this area is essential for developing effective and scalable biodegradation solutions to address the challenges posed by plastic waste, including PU[11-13].

Exactly, in the biodegradation process, researchers have discovered that certain microbes can survive in environments containing polyurethane. This observation suggests the possibility that these microbes could actively utilize PU as a substrate for their metabolic processes. The microbial activity involved in breaking down PU is a key area of interest in the development of biodegradation solutions for managing plastic waste more sustainably. The degradation process of PU begins with microbial adhesion to the polymer surface, leading to the development of a biofilm[14]. This biofilm formation appears to be essential for effective biodegradation to occur[15]. Therefore, the PU

surface is a very crucial factor for biodegradation of polymers. The process of PU micronization can occur as PU degrades in the environment, breaking down the polymer into micro-particles commonly known as micro plastics. Despite the increasing health and environmental concerns associated with micro plastics[16], their extensive surface area facilitates the easier accessibility of degrading enzymes and microorganisms.

Harnessing the natural capabilities of microorganisms to degrade PU could offer a promising avenue for reducing the environmental impact of this widely used material[17]. The reported genera of some bacteria capable of breaking down PU polymers include Pseudomonas, Comamonas, Bacillus, and Acinetobacter[18,19]. A study conducted by Peng et al.[19] demonstrated that *Pseudomonas putida*, when provided with PU as the sole carbon source, exhibited the ability to break down 92% of the PU substrate within four days at 30 °C. This finding was subsequently confirmed through Fourier Transform Infrared (FTIR) analysis. Additionally, various fungus genera, such as Aspergillus, Pestalotiopsis, Cladosporium, Fusarium, and Penicillium, have been identified with biodegradation capabilities for PU[20].

The enzymatic degradation of PU has been thoroughly examined. There are several factors and conditions such as substrate specificity, optimum temperature and pH that determine the maximum activity of the enzyme[21]. Among the various enzymes involved, the protease enzyme has shown promising results with PU[22,23]. The optimum pH and the optimum temperature of protease required for degradation of PU are 7[24] and 32 °C, respectively[25]. The degradation of PU follows a sequence: first, the urethane linkages undergo degradation; next, there is a reduction in the molecular weight and viscosity of the PU; and finally, all PU polymer chains are degraded, as outlined in the study by Mahajan and Gupta in 2015[9]. In a study by Howard and Blake[26], a polyurethane-degrading enzyme, protease, was discovered in *Pseudomonas fluorescens*. The bacteria, when inoculated in a polyester PU as the sole carbon and energy source, demonstrated the capability to hydrolyze the PU. This activity resulted in 2 cm zones of clearing at 25 °C and pH 5. According to previous studies, protease gave promising results in the biodegradation process. Therefore, the protease enzyme was used in our investigation. Among different types of PU, PU-HDI and PU-IPDI are the common type of aliphatic diisocynate based PU in various applications[27,28].

However, the exact binding pocket of the protease enzyme, as well as the interactions between the protease enzyme and PUs are still not fully identified. Therefore, building on insights from previous studies, this work focused on studying the initiation step of the PU degradation process. Therefore, the binding site and binding interactions between the two polyester PUs, PU-HDI and PU-IPDI, with the protease enzyme from *Pseudomonas sp* were identified and it was analyzed through various computational techniques. Chemical reactivities of PU-HDI and PU-IPDI with protease enzyme were also identified by the present work.

2. Materials and methods

2.1 *Homology modeling of protease enzyme*

The primary amino acid sequence consisting of 587 amino acids of the protease enzyme from *Pseudomonas sp*, was retrieved from the Uniprot server (uniprot ID: P42790)[29]. The complete 3D structure of protease enzymes was determined by Iterative Threading Assembly Refinement (I-TASSER) web server[30]. The given sequence of the target protein is aligned with the homologus structures available on the Protein Data Bank (PDB) to develop the secondary structures in the protease enzyme. The selection of the best structure is based on the c-score which measures confidence of the model calculated by considering the significance of treading template alignments and convergence parameters of the structure assembly simulations[30].

2.2 *MD simulations and the validation of the protease model*

The selected protein model of protease was protonated at pH 7 by Propka server[31] to assign the correct protonation states for the amino acids as pH 7 is the optimal pH of protease enzyme[32]. To analyze the structural stability of the modeled protease enzyme in the aqueous medium, 150 ns long MD simulations were carried out using Nanoscale Molecular Dynamics (NAMD) software package[33]. The CHARMM-GUI server was used to prepare the input files for MD simulations of modeled protein via NAMD[34]. The protease enzyme was solvated by using the TIP3P water model in a 10 Å cubic water box before a short minimization with the Steepest Descent algorithm[35] followed by the Adopted Newton Raphson algorithm[36]. The system was neutralized by adding 5 Na^+ as the solvated system contains a charged

protein. The equilibrium was performed in the Number of particles, Volume, and Temperature (NVT) phase for 1ns while dynamics was run for 150 ns with a 2 fs time step with the NPT phase. Both equilibrium and dynamic steps ran with a temperature of 310 K using the Verlet algorithm. Long-range electrostatics were calculated via Particle Mesh Ewald[37].

2.3 *Tunnel analysis and the binding pockets analysis of protease*

So far, the exact amino acid composition of the binding site of protease enzyme has not been discovered yet. However, some binding residues in the binding pocket were identified in the literature. In order to identify the exact composition of the binding site that PU models (PU-HDI and PU-IPDI) interact with, the tunnel analysis and the binding pocket analysis were carried out. This has been accomplished by Cavity and Tunnel Analysis (CAVER) analyst 2.0[42] and it uses the additive weighted Voronoi diagrams theory to calculate the tunnels[43]. The following parameters were set to calculate the tunnels: probe radius of 1.4 Å, and shell depth of 4 Å, shell radius of 3 Å. The binding pockets of the protease enzyme were determined by the DoGSiteScorer. After determining tunnels and pockets, the most preferred tunnel and the pocket were selected by comparing the amino acid composition of each amino acid and the identified binding residues.

2.4 *Molecular docking studies*

Both PU-HDI and PU-IPDI are aliphatic PU-models that are used in the molecular docking process. The two PU models were modeled using GaussView 4.1[44] and optimized using b3lyp 6-31G (d,p) level of theory[45] by Gaussian 16[46] prior to docking calculations. The modeled protease enzyme and both PU models were prepared for docking calculations by using Autodock 4.2 software package[47]. Autogrid module was used to construct the grid map for the selected tunnel which resulted from a tunnel analysis. Then docking of both PU models was carried out to the selected binding site via AutoDock[47] after placing the grid box. The Lamarckian Genetic Algorithm[48] was employed to generate 10 poses for each polymer docking. Finally, a pose that forms a a higher number of H-bonds with higher docking score value was selected for MD simulations for each PU model.

2.5 *The chemical reactivity of PU*

The Natural Bond Orbital Analysis (NBOA)[49] was conducted through the application of second-order perturbation theory, utilizing the NBOA module within the Gaussian16 package. Fukui functions (f+, f-, f0) and Dual Descriptor (DD) values were computed for every atom in both cis and trans isomers employing the UCA Fukui software package[50]. The DD parameter effectively combines the Fukui functions f+ and f-[51], offering a more comprehensive depiction of the nucleophilic and electrophilic tendencies of the atomic centers.

2.6 *MD simulations of protease-PU complex*

Each aliphatic PU model bound to the proposed binding site in protease enzyme was further validated through 150 ns MD simulations. The topology and parameters for the protease enzyme and the PU models were prepared via the CHARMM-GUI web server[31]. Both complexes were simulated with CHARMM36 force field[52] by using the NAMD software[33] package. For each complex, the TIP3P water model was used to solvate the complex in a 10 Å rectangular water box while neutralizing the charged complex with 6 Na^+. Monte-Carlo method[53] was used as the ion placing method for the neutralization step. Periodic boundary conditions are set for each complex after a short minimization carried out by Steepest Descent and Adopted Newton Raphson algorithm[36]. Each system was equilibrated in the aqueous medium with an NVT ensemble for 125 ps while running the dynamics simulations for 150 ns in the NPT ensemble. The time scale that is used for NVT, NPT equilibration and dynamics step is 2 fs. The electrostatic interactions were calculated by using the Particle Mesh Ewald[37] method.

The interacting hydrogen bonds between the aliphatic PU model in both complexes and binding residues in the binding pockets were analyzed throughout the 150 ns MD simulations using the Visual Molecular Dynamics (VMD) software[54] package. The occupancy of the hydrogen bond formed by amino acids residues with carbonyl carbons

present in both aliphatic PU models were investigated. Employing short MD simulations with the Gromacs software package, the determination of interaction free energy between the PU model and proteins made use of the MM/PBSA methodology[55].

3. Results and discussion

3.1 *Structure of polyurethane from HDI and IPDI monomers*

The structures of PU-HDI and PU-IPDI have a common soft segment, consisting of a polybutylene adipate group. However, their hard segments differ; PU-HDI incorporates 1,6-Hexamethylene diisocyanate, while PU-IPDI includes 5-isocyanato-1-(isocyanatomethyl)-1,3,3-trimethylcyclohexane as the aliphatic diisocyanate segments. Atom numbered structures are given in Figure 1. The molecular weight of the modeled PU-HDI is 290.36 g/mol, while the modeled PU-IPDI has a molecular weight of 204.23 g/mol. The two models consist of 76 atoms and 86 atoms, respectively. The modeled structures of PU-HDI and PU-IPDI models were optimized using DFT b3lyp/6-31G (d, p) level of theory. The molecular length of PU-HDI is 36.577 Å, and PU-IPDI is 42.572 Å.

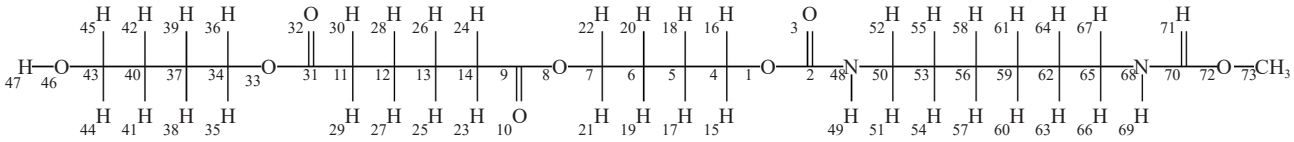

(a)

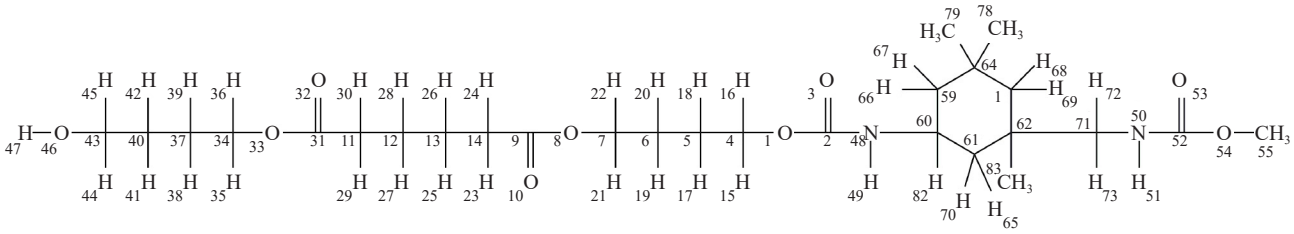

(b)

Figure 1. 2D structures of (a) PU-HDI and (b) PU-IPDI

Both PU-HDI and PU-IPDI models show bent configuration as shown in Figure 2. As a result, it can be argued that both polymer chains can have a zigzag conformation, and it can be significantly impact the packing arrangement of molecular chains in the polymer matrix.

Quantum mechanical frequency calculations (Appendix 1) indicated that there are no imaginary frequencies, suggesting that the resulting structures have a stable ground state configuration. Based on the conformation of the urethane group previous studies have shown that the trans structure of PU is more stable in the ground state than the cis structure[56]. Therefore, in the study, both models were selected in the form of trans configuration for further investigation.

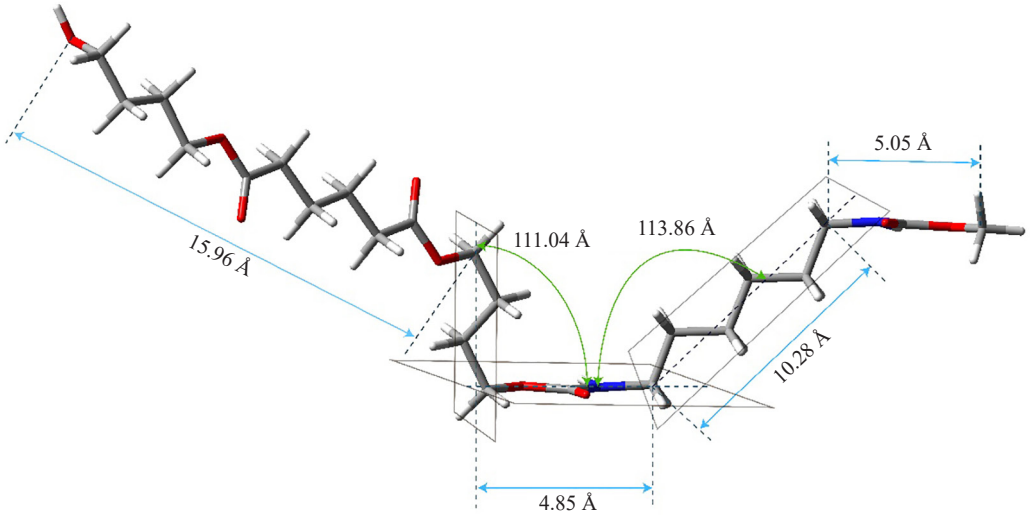

(a)

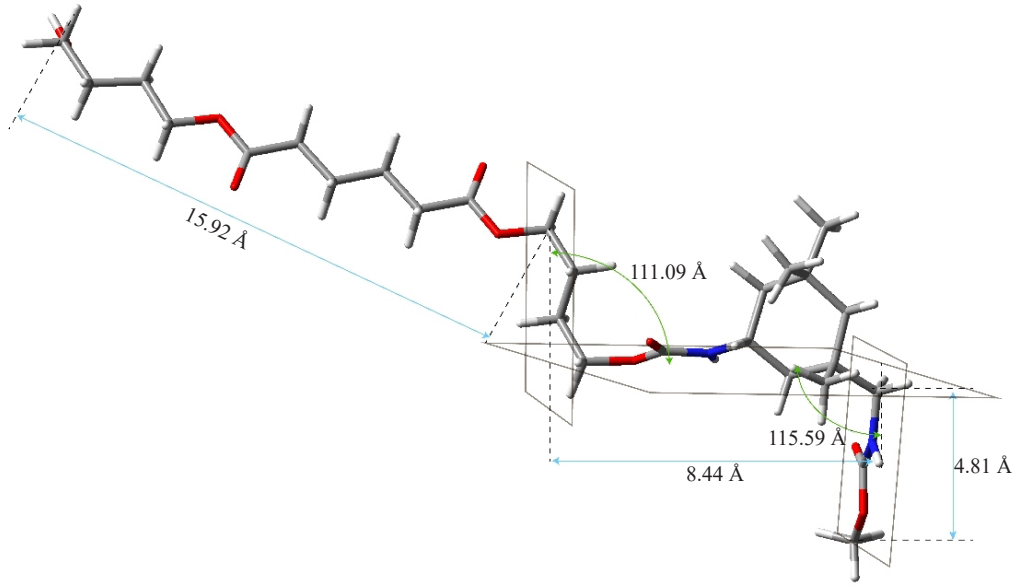

(b)

Figure 2. DFT optimized structures of (a) PU-HDI and (b) PU-IPDI modeled compounds

3.2 *Modeling and validation of protease enzyme*

The protease enzyme is composed of 587 amino acids. However, the 3D structures of protease enzymes found in the PDB database are incomplete, lacking certain amino acids. Therefore, the 3D structure of protease was modeled using a technique known as homology modeling. Homology modeling is a computational technique to predict the 3D structure of a protein based on the known structures of related homologous proteins that have similar amino acid sequences[57].

There are seven steps in homology modeling; Template identification from the protein database and initial amino acids sequence alignment, Alignment correction, the formation of protein backbone, loop modeling, side-chain modeling, optimization of model structure and structure validation[58]. Thus, proposing a comprehensive model became necessary, and this has been accomplished using an approach based on secondary structure-enhanced Profile-Profile

Threading Alignment (PPA) through the I-TASSER server[30]. The construction of the 3D structure of the protease enzyme involved the selection of the following PDB hits based on threading alignment and their respective Z scores: 1TLEA (chain A, 28%), 7V7Y (chain A, 15%), 1GA6 (chain A, 63%), and 7DRR (chain D, 24%). The C-score can be described as a confidence score that is used to predict the structural superiority of 3D model structures[59]. This is computed by the convergence parameters of the structure assembly simulations and the importance of threading template alignments. Typically, the C-score varies between -5 to 2 where a higher C-score indicates greater confidence in the model[59]. From the modeled structures, which exhibited C-scores spanning from -0.98 to -2.28, the structure with the highest C-score (-0.93) was chosen as the most fitting model for the protease. Figure 3 illustrates the cartoon representation of the proposed model for the protease enzyme. Z score is defined as the difference between the raw and average score in the standard deviation. Among these hits, 1TLE had the highest Template Modeling score (TM-score) of 0.88, which evaluates the topological similarity between proteins.

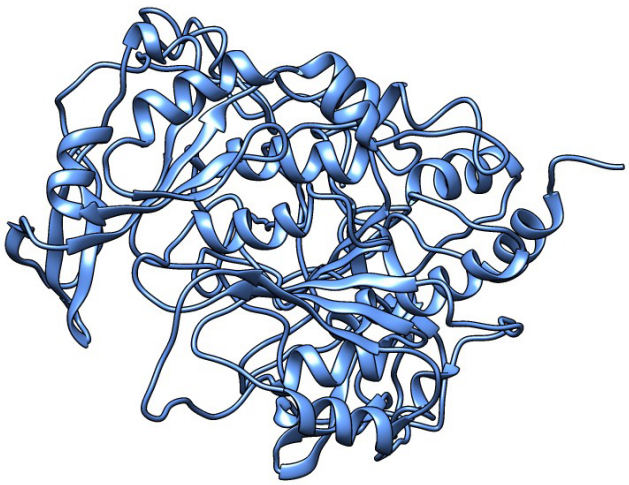

Figure 3. The cartoon representation of modeled structure of protease enzyme

MD simulations were employed to study the structural stability of the modeled protease enzyme in an aqueous medium. The simulation duration spanned 150 ns, utilizing the CHARMM36 force field[60]. Concerning the root mean square deviation (RMSD) plot presented in Figure 11 (d), the modeled protease enzyme reached an equilibrium conformation approximately after 40 ns. To assess the quality and accuracy of the modeled protease enzyme, various structure validation tools and stereo chemical analysis tools, including PROCHECK[61], verify3D[41], ProSA[39], and ERRAT[40], were employed. The last frame of the protein trajectory was utilized for this analysis, and a summary of the stereochemical analysis results is provided in Table 1.

The most common stereochemical analysis tool is the Ramachandran plots. The Ramachandran plots were created using the PROCHECK server[61] for both structural states (pre and post-MD simulations) and were compared (Figure 4a). In the structure, after MD simulations, 86.30% of residues shifted to the most allowed region compared to the initial structure. Furthermore, the percentage of residues in the disallowed region was reduced to 0.2%, confirming that the predicted model attained a more energetically stable conformation after the MD simulation process.Verify3D is another stereochemical analysis tool and it was used to obtain the 3D profile of the protease enzyme[41], confirming that 80.17% of residues achieved an average score equal to or greater than the threshold value of 0.1 (Figure 4b). This suggests that the model's quality is acceptable. The ERRAT score generated for the protease was 90.337, indicating a high-quality model. Residues exceeding the 95% error limit indicate that misfolded regions are not associated with residues in the binding pocket. The Z-score from ProSA, where experimentally determined structures generally range from +10 to -20, was -7.24 for the modeled structure of proteases. Due to the respective negative energy values, the energy values plotted against the amino acid sequence confirm that the majority of residues are correctly modeled.

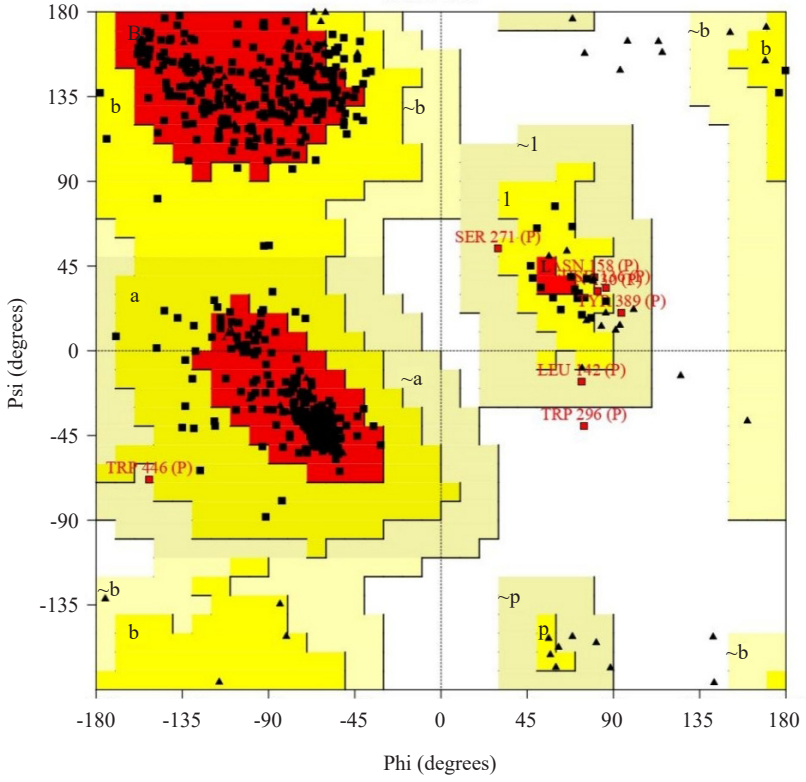

(a)

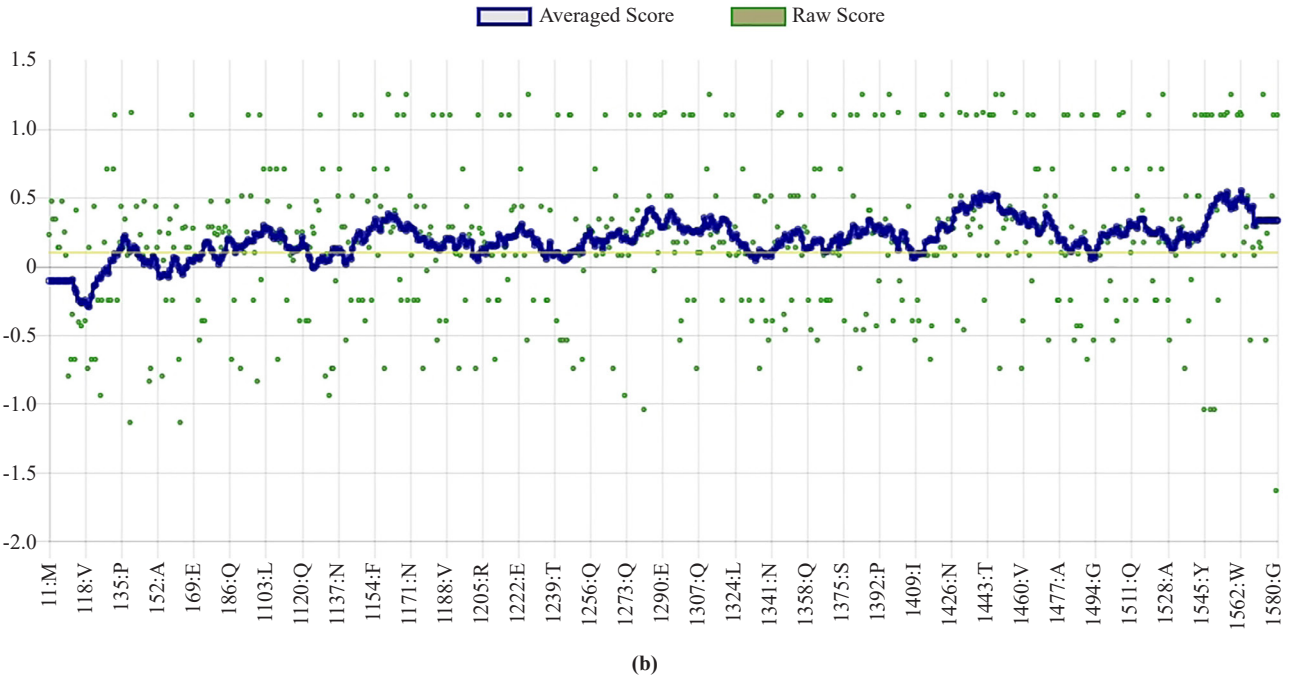

(b)

Figure 4. (a) The Ramachandran plot and (b) Verify 3D graph of protease enzyme

Table 1. Summary of the structure validation analysis results of the modeled structure of the protease enzyme

Model State	Ramachandran plot-Residues in the most allowed region	ERRAT-Overall quality factor	Verify3D-Averaged 3D-1D score	ProSA-Z-score
Before the MD	63.20%	80.95%	79.14%	-5.99
After the MD	86.30%	90.06%	80.17%	-7.24

3.3 *Binding site analysis*

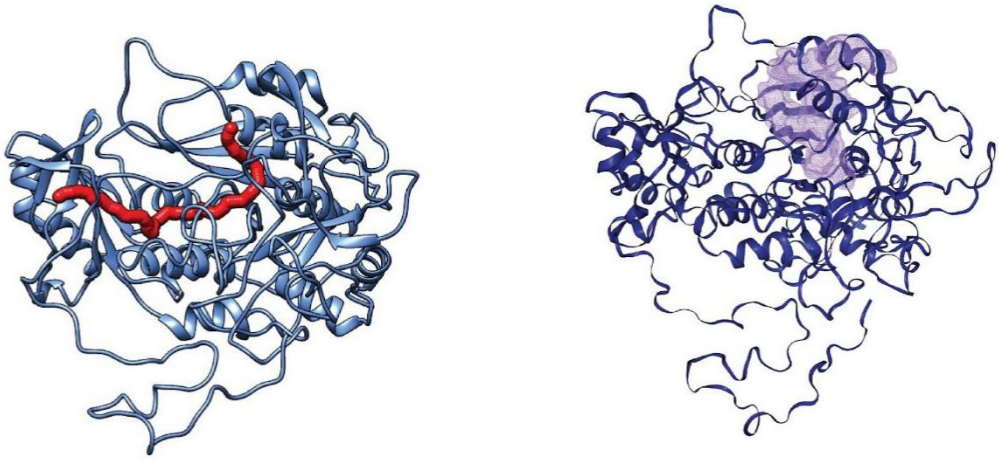

(a) (b)

Figure 5. (a) The binding tunnel shown in red color and (b) the binding pocket of the protease

The initiation of the catalytic mechanism of PU degradation occurs when the PU linkages bind to the active site of the protease enzyme. The complete amino acid composition of the binding pocket in the protease enzyme remains undisclosed. However, in a study by Wlodawer et al.[62], GLU295, ASP299, ASN346, SER348, ASP385, GLY499, THR501, and SER502 were identified as binding residues using a potential covalent inhibitor. In this investigation, a comprehensive analysis of the potential binding site of the protease enzyme was conducted, utilizing both tunnel and pocket analysis. Seven primary potential tunnels and ten possible binding pockets were identified. Pockets and tunnels details are shown in Appendix 2. The most favorable tunnel and binding pocket were determined by comparing the previously mentioned binding residues within each tunnel and pocket. It can be argued that the selected tunnel exhibits more hydrophobic characteristics as it is situated inside of the protein structure.

The statistics of the selected tunnel were evaluated in terms of length, bottleneck radius, and curvature. The bottleneck radius represents the narrowest part of the tunnel, the length indicates how deep the tunnel extends through the protein, and the curvature is the shape determined by the ratio between the length of the tunnel and the difference between the starting and ending points of the tunnel. The selected tunnel has a length of 62.66 Å, a bottleneck radius of 0.91 Å, and a curvature of 7. The existence of the selected tunnel was further validated through the GHECOM 1.0 server by confirming all the residues found in the selected tunnel are within the same pocket[63]. The result from the GHECOM 1.0 server is illustrated in Appendix 3, with respect to the identified binding residues for the selected tunnel through the tunnel analysis. The 3D grid representation confirms the existence of the pocket, and it further confirms the residues in the selected tunnel are located in more hydrophobic deeper inside of the protein molecule due to the higher pocket score value (the higher pocket score, the deeper the residue, Figure 5).

3.4 *Polymer binding and dynamics stability of protein-polymer complex*

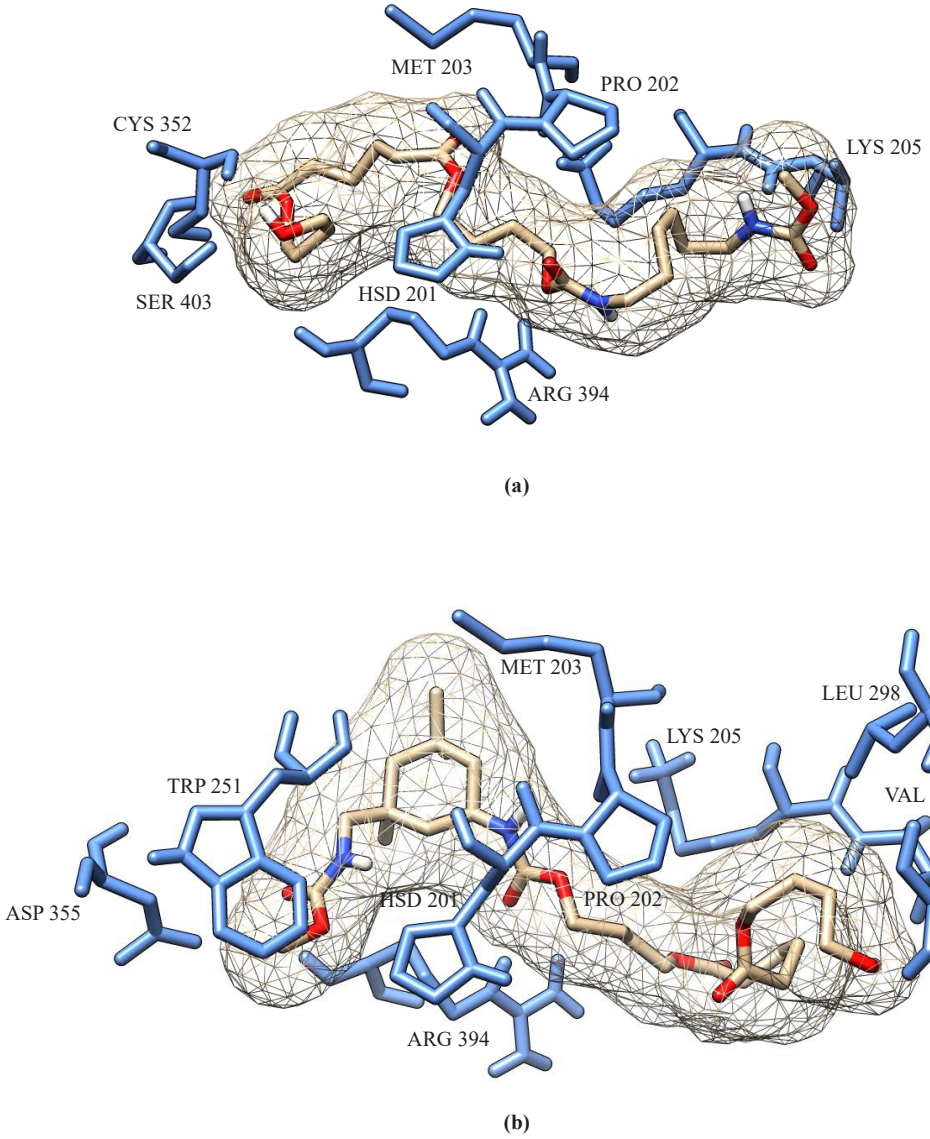

Figure 6. Illustration of the amino acid interactions observed between the protease enzyme and the PU-HDI (a) and PU-IPDI (b) models compounds

The modeled structures of PU-HDI and PU-IPDI were used to explore enzymatic degradation possibilities for aliphatic PU. Docking studies for both aliphatic PU models were conducted using the AutoDock software[47]. The 2D polymer-protein interaction plots for each pose were obtained via Discovery Studio[64]. The poses with the highest binding affinity for both aliphatic PU models were selected based on the hydrogen bonds interactions formed between the urethane linkage and potential amino acids. PU-HDI binds to the protease with a binding affinity of -5.7 kcal/mol, while PU-IPDI binds with -6.9 kcal/mol. The selection of the best possible pose for the enzyme-PU complex took into account both the binding affinity of PU towards the protease enzyme and the hydrogen bond interactions between the urethane linkage and the protease enzyme (Figure 6). Figures of each pose of PU-HDI and PU-IPDI are represented in Appendix 4.

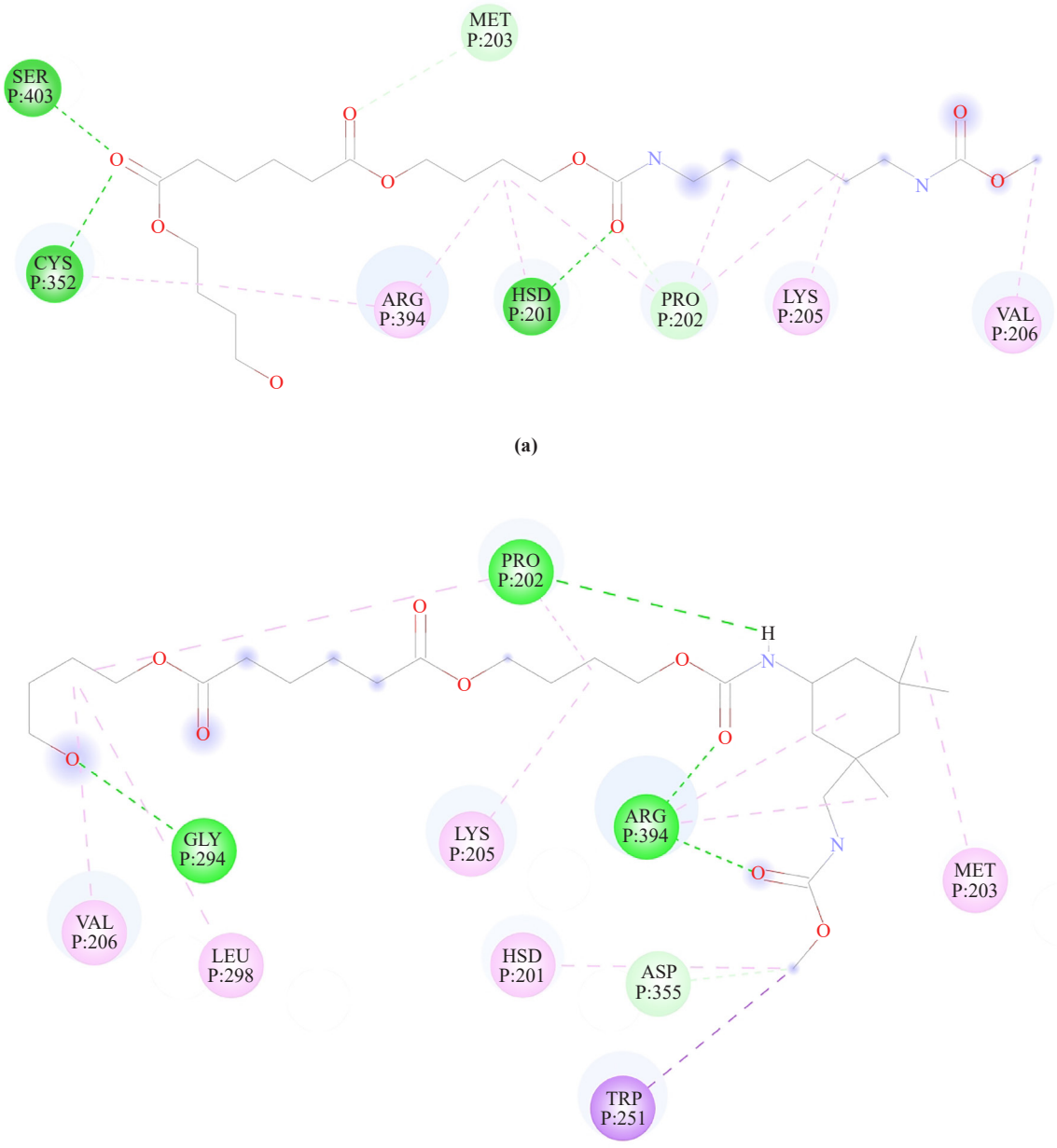

Figure 7. The 2D interactions diagram of the (a) PU-HDI and (b) PU-IPDI with protease modeled enzyme

Therefore, this study gives important findings on the binding interactions that occur between PU-IPDI and PU-HDI polymers and protease enzymes. With this knowledge, polymers that are more prone to enzymatic degradation can be designed and it could lead to the creation of environmentally useful biodegradable material.

3.5 *The chemical reactivity of PU*

The chemical reactivity of both PU-HDI and PU-IPDI were estimated through the calculating Fukui reactive indices alongside the corresponding dual descriptor (DD) values[50]. The Fukui function elucidates alterations in electron density within a frontier orbital resulting from a slight variation in the total number of electrons. To express it more formally, the Fukui function represents the first derivative of electron density concerning the number of electrons, while maintaining a constant external potential[65]. The electron density discontinuity leads to the emergence of three distinct derivatives: f+ for nucleophilic attack, f- for electrophilic attack, and f0, which measures the radical reactivity. Figure 8 and Figure 9 illustrate the Fukui functions f+, f-, f0 and their corresponding DD values for PU-HDI and PU-IPDI respectively. For a comprehensive overview, the values of Fukui functions and DD values for both PU-HDI and PU-IPDI are provided in Appendix 5. While the individual Fukui functions can anticipate local reactivities, research has demonstrated[56,66] that the dual descriptor (DD) values offer a more precise depiction of local nucleophilicity and electrophilicity.

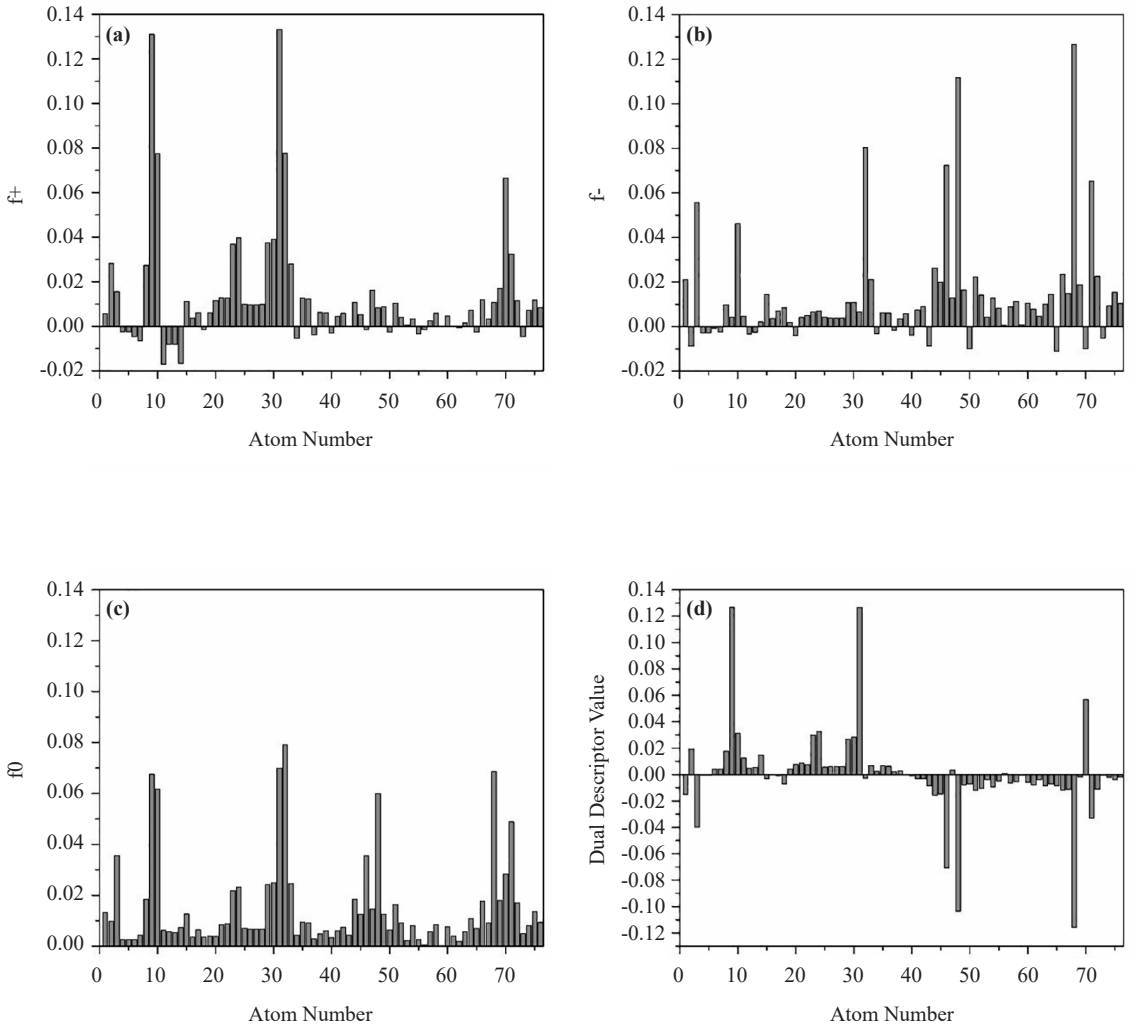

Figure 8. (a) Positive Fukui function (f+), (b) Negative Fukui function (f-), (c) Fukui function (f0) and (d) Dual descriptor values of PU-HDI

As shown in Figure 8 the DD values indicate that in PU-HDI, positions C2, C9, C31, and C70 exhibit greater

susceptibility to nucleophilic attacks due to their higher positive DD values. Conversely, positions O3, C46, N48, and N68 display a preference for electrophilic attack, as evidenced by their negative DD values. Specifically, among these positions, C9 and C31 stand out with the highest tendency for nucleophilic attack, possessing DD values of 0.1268 and 0.1266 respectively. While N68 exhibits the highest tendency for electrophilic attack, gaining a DD value of -0.1157. In PU-IPDI, atomic positions C9, C31, and C70 are identified as more prone to nucleophilic attacks due to their higher positive DD values as shown in Figure 9. Conversely, atomic positions O3, C46, N48, and N50 exhibit a greater probability for electrophilic attack, characterized by their negative DD values. Analysis of the DD values for PU-IPDI reveals that C9 and C31 positions notably demonstrate the highest tendency for nucleophilic attack, with DD values of 0.119 and 0.1225 respectively. Whereas the N48 atomic position showcases the highest chance for electrophilic attack, with a DD value of -0.1255.

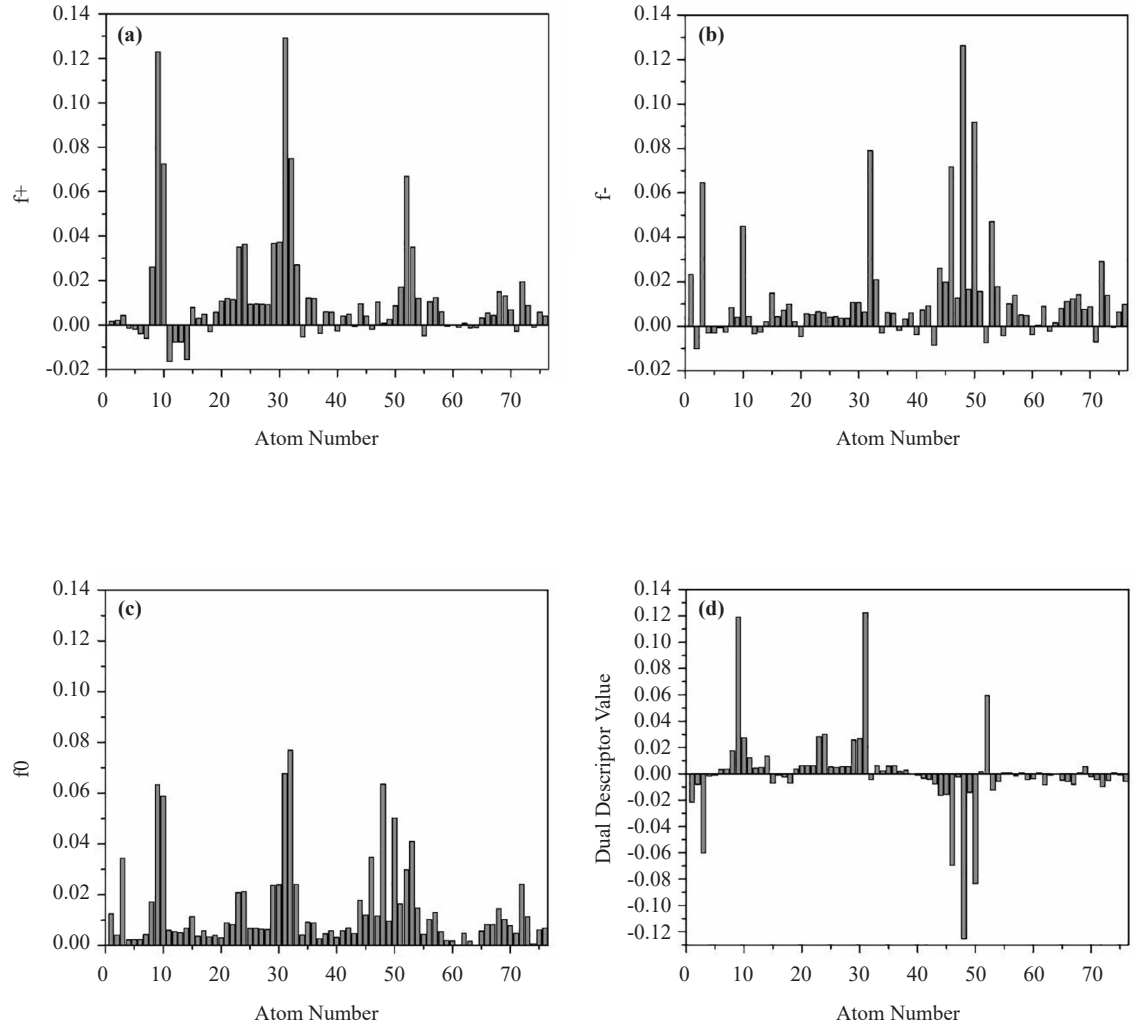

Figure 9. (a) Positive Fukui function (f+), (b) Negative Fukui function (f-), (c) Fukui function (f0) and (d) Dual descriptor values of PU-IPDI

As depicted in Figure 8 and Figure 9, the urethane linkage emerges as the most probable site for the initiation of degradation. As well as Figures 7(a) and 7(b) illustrate both hydrophobic and hydrophilic interactions between each PU and the protease enzyme. It reveals that PU-HDI formed a total of 13 inter molecular interactions, including three hydrogen bond interactions, one pi-alkyl bond interaction, eight alkyl bond interactions, and one carbon-hydrogen

bond interaction. PU-IPDI engaged in a total of fifteen intermolecular interactions, comprising four hydrogen bond interactions, nine hydrophobic interactions, one pi-sigma bond and one carbon Hydrogen bond. The initiation of enzyme catalytic degradation heavily relies on the potential of binding polymer to the enzyme. This can lead to weak bonds in the PU short chains, making them more susceptible to degradation. Hence, it is essential to investigate the atomic bond parameters of PU, in before and after MD simulations. Table 2 presents the changes in all the bond lengths of urethane linkages in both PU models.

Table 2. Bond lengths of urethane linkages in PU-HDI and PU-IPDI

Bond Number	Bond lengths in PU-HDI/Å		Bond Number	Bond lengths in PU-IPDI/Å	
	Before MD simulations	After MD simulations		Before MD simulations	After MD simulations
C4-O1	1.44	1.43	C4-O1	1.44	1.46
O1-C2	1.37	1.32	O1-C2	1.37	1.40
C2-O3	1.22	1.20	C2-O3	1.22	1.23
C2-N48	1.36	1.38	C2-N48	1.36	1.36
N48-H49	1.01	1.00	N48-H49	1.01	0.99
N48-C50	1.46	1.42	N48-C60	1.48	1.48
C65-N68	1.45	1.40	C71-N50	1.45	1.43
N68-H69	1.01	1.00	N50-H51	1.01	0.99
N68-C70	1.36	1.33	N50-C52	1.36	1.38
C70-O71	1.22	1.24	C52-O53	1.22	1.25
C70-O72	1.36	1.39	C52-O54	1.36	1.31
O72-C73	1.43	1.41	O54-C55	1.43	1.42

Upon comparing these results, the bond length between C and O in the carbonyl carbon of the urethane linkage emerged as the site where degradation occurs. Specifically, the bond lengths of C2-N48, C70-O71, and C70-O72 in PU-HDI positions increased from 1.36 Å to 1.38 Å, from 1.22 Å to 1.24 Å and from 1.36 Å to 1.39 Å, respectively whereas in PU-IPDI the bond length of C4-O1, C2-O3, and N50-C52 increased from 1.44 Å to 1.46 Å, from 1.22 Å to 1.23 Å, and from 1.36 Å to 1.38 Å, respectively. Given the significant weakening of these bonds after the MD simulations, it can be argued that these bonds serve as initiation sites for the degradation of these two polymer short chain models. The dynamic stability of the complex formed by the PU model and the protease enzyme was examined through a 150 ns long MD simulations using the NAMD software package[33]. An MD simulation's trajectory is a 3D representation of the atomic level changes of a system with respect to time. These simulations provide very accurate information about the position and motion of each atom at any given time, tunnels which are located is highly challenging to obtain from experimental chemistry. The trajectory of the protease-PU complexes confirmed the stability of both PU models, remaining within the binding pocket without deviation. The RMSD, RMSF, flexibility analysis, and H bond analysis were investigated using the trajectory of protease-PU complexes. The RMSD plots for both complexes are depicted

in Figure 11, and both achieve a stable configuration within the initial 40 ns, aligning with expectations of reaching equilibrium.

Further analysis involved studying the dynamic stability of hydrogen bond interactions between PU models and the protease enzyme, crucial for maintaining the complex stability throughout the trajectory. The hydrogen bond interactions over the 150 ns MD trajectory for both complexes are illustrated in Figure 10.

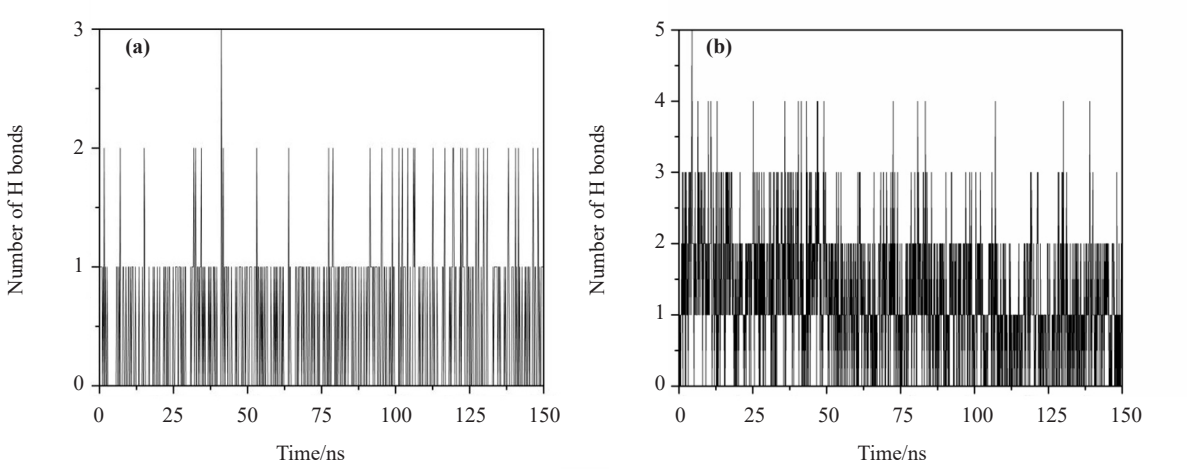

Figure 10. Number of hydrogen bonds between protease and (a) PU-HDI and (b) PU-IPDI

As depicted in Figure 10, it is evident that, during the MD simulations of the PU-HDI and PU-IPDI, up to Figure 11, three hydrogen bonds and five hydrogen bonds respectively, can be observed with the protease enzyme at certain instances, although the majority of hydrogen bonds occur in between one and two. The prevailing scenario indicates the maintenance of one or two hydrogen bonds throughout the simulation period. Notably, the occupancy of hydrogen bond interactions between PU-IPDI and the protease enzyme is significantly higher than that between PU-HDI and the protease enzyme. However, the continuous formation of hydrogen bonds in both complexes throughout the entire trajectory suggests strong interactions between the polymer and the enzyme. This high tendency to initiate the degradation of PU is attributed to the crucial role of the interaction between PU and the enzyme in the initiation step of PU degradation.

Throughout the MD simulations, PU-HDI exhibits hydrogen bond interactions between urethane linkages and ARG57, ASN393, VAL206, THR198, TYR164, SER58 in the protease enzyme (Table 3). The highest occupancy of hydrogen bond interaction in the urethane linkage is observed in PU-HDI with ARG57. Similarly, PU-IPDI displays its highest occupancy with ARG394. These results underscore a robust binding affinity for both PU-IPDI and PU-HDI with the protease enzyme, emphasizing their significant contribution to the initiation of degradation mechanisms.

Table 3. H-Bond occupancy of urethane linkage of PU-HDI and PU-IPDI

Atom Number	H-bond occupancy of PU-HDI	Atom Number	H-bond occupancy of PU-IPDI
O3	ARG57-2.40% VAL206-0.93% TYR164-0.53% THR198-0.40% ASN167-0.40% LYS444-0.13% HSP201-0.13% SER58-0.13%	O3	ARG394-42.80% LYC205-0.13% ARG394-0.07%
N48	THR198-0.53% ASN393-0.40% GLU55-0.27% GLU295-0.13% ARG57-0.13% ASN167-0.13%	N48	PRO202-37.06%
N68	PRO202-0.53% ASN393-0.40% TRP351-0.13% HSP201-0.13% ASP355-0.13%	N50	-
O71	ARG57 0.40% ASN393 0.13%	O53	HSD201-18.80%

3.6 *Stability and flexibility of protease upon polymer binding*

The flexibility of the modeled protease enzyme was further assessed using MDLovofit and calculating the Root Mean Square Fluctuation (RMSF). Results from the MDLovofit program, the red color signifies the most flexible regions of the protein, while blue indicates rigid segments as illustrated in Figure 11 (a), Figure 11 (b) and Figure 11 (c). Upon the binding of PU-HDI and PU-IPDI, it was observed that the flexibility of the protease enzyme slightly decreased, as evident from the shift in color from red to blue in the region where the polymer binds.

Upon comparing the RMSF plot for the protease enzyme with both PU-HDI and PU-IPDI model complexes, it is evident that the modeled PU models significantly influence the flexibility of the protease enzyme. The RMSF graphs for both complexes illustrate a notable decrease in fluctuation among all the binding residues present in the binding pocket compared to those binding residues in the protease without the PU models. This further confirms the efficacy of the

protease enzyme in initiating the degradation of PU-HDI and PU-IPDI models. While the results of this study indicate that the protease enzyme is more effective in binding PU-IPDI compared to the PU-HDI model, further investigation is required to study the reaction kinetics of the mechanisms involved in the degradation of these two aliphatic PU models. However, this study evaluates the stability of the polymer-enzyme complexes, which can be used for determining the feasibility and effectiveness of enzymatic degradation in real-world applications.

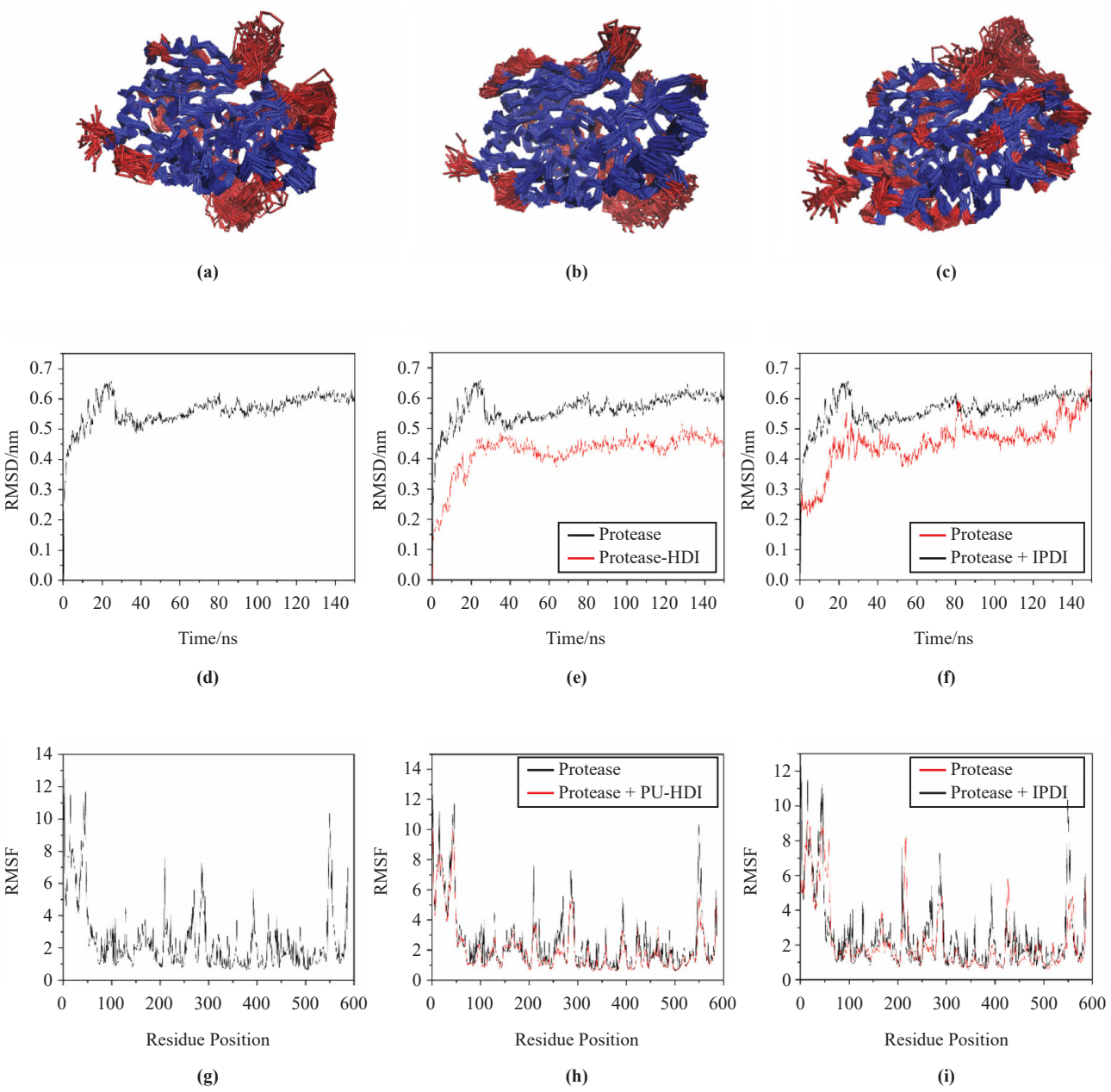

Figure 11. (a) The flexibility of the free protease compared to its complex with (b) PU-HDI and (c) PU-IPDI. Regions displaying higher flexibility are depicted in red, while more rigid regions are shown in blue. RMSD of amino acid residues for (d) the free protease is depicted in black, while in the complex with (e) PU-HDI and (f) PU-IPDI, it is represented in red. RMSF of C-alpha atoms is depicted in black for (g) the free enzyme, and in red for the complexes with (h) PU-HDI and (i) PU-IPDI

As shown in Table 4, the interaction free energy between Protease and PU-HDI and PU-IPDI models were

investigated by using the MM/PBSA methodology. It was indicated that the interactions between the PU models and the protease enzymes are indeed strong, -8.368 $kJmol^{-1}$ for the complex with the PU-HDI and -89.99 $kJmol^{-1}$ for PU-IPDI, verifying the findings derived from the analysis of both structure and dynamics. It further proved the significant effectiveness of protease enzyme for the degradation of PU-IPDI polymer segment compared to the PU-HDI.

Table 4. Interaction free energies between protease and PU models

System	Van der Waals energy (kJ/mol)	Electrostatic energy (kJ/mol)	Total energy (kJ/mol)
PU-HDI	-224.01 ± 1.67	-60.79 ± 10.66	-8.368 ± 4.72
PU-IPDI	-199.78 ± 4.85	-146.31 ± 5.18	-89.99 ± 6.69

4. Conclusion

The enzymatic degradation methods for micro plastic materials have garnered increasing attention in scientific research. However, a comprehensive understanding of the intricate interactions between enzymes and non-natural substrates is still lacking. In this study, molecular dynamics was employed to investigate the protease from *Pseudomonas sp*, along with both PU-HDI and PU-IPDI, shedding light on their structural characteristics and interactions with the protease enzyme. RMSD analysis revealed stability across all systems. Modeled PU-HDI and PU-IPDI exhibited consistent H bond interactions with the enzymes, forming at least one hydrogen bond over the 150 ns simulations period. Both polymers-maintained proximity to their initial positions, displaying robust interactions throughout the simulations, with the interaction free energies between the enzyme and the PU-HDI (-8.368 ± 4.72 kJ/mol.) and PU-IPDI (-89.99 ± 6.69 kJ/mol) proving to be notably strong. The results from this study offer detailed insights into the interactions between PU-HDI and PU-IPDI with the enzyme. By understanding the enzymatic degradation mechanisms, the study could cover the way to developing biodegradable polyurethanes, reducing environmental pollution from plastic waste. Furthermore, the QM/MM studies on both polymer-protease complexes are suggested for a deeper exploration of the reaction kinetics involved in the biodegradation process. The findings of this study contribute to the broader field of sustainable materials, supporting the transition to more environmentally friendly products in various industries.

Acknowledgments

High-performance computing facilities were provided by the Centre for High-Performance Computing (CHPC) Council for Scientific and Industrial Research, National Integrated Cyber Infrastructure, Cape Town, Republic of South Africa.

Conflict of interest

The authors declare no competing financial interest.

References

[1] Skleničková, K.; Abbrent, S.; Halecký, M.; Kočí, V.; Beneš, H. Biodegradability and ecotoxicity of polyurethane foams: A review. *Crit Rev Env Sci Tec.* **2022,** *52*(2), 157-202.
[2] Tomin, M.; Kmetty, A. Polymer foams as advanced energy absorbing materials for sports applications-A review. *J. Appl. Polym. Sci*. **2022,** *139*(9), 51714.

[3] Liang, C.; Gracida-Alvarez, U. R.; Gallant, E. T.; Gillis, P. A.; Marques, Y. A.; Abramo, G. P.; Hawkins, T. R.; Dunn, J. B. Material flows of polyurethane in the United States. *Environ. Sci. Tech*. **2021,** *55*(20), 14215-14224.
[4] Fangareggi, A.; Bertucelli, L. Thermoset insulation materials in appliances, buildings and other applications. In *Thermosets*; Woodhead Publishing, 2012; pp 254-288.
[5] Sambasivam, M.; White, R.; Cutting, K. Exploring the role of polyurethane and polyvinyl alcohol foams in wound care. In *Wound Healing Biomaterials*; Elsevier, 2016; pp 251-260.
[6] Liu, J.; He, J.; Xue, R.; Xu, B.; Qian, X.; Xin, F.; Blank, L. M.; Zhou, J.; Wei, R.; Dong, W. Biodegradation and up-cycling of polyurethanes: Progress, challenges, and prospects. *Biotechnol. Adv.* **2021,** *48*, 107730.
[7] Osman, M.; Satti, S. M.; Luqman, A.; Hasan, F.; Shah, Z.; Shah, A. A. Degradation of polyester polyurethane by Aspergillus sp. strain S45 isolated from soil. *J. Environ. Polym. Degrad.* **2018,** *26*, 301-310.
[8] Lucas, N.; Bienaime, C.; Belloy, C.; Queneudec, M.; Silvestre, F.; Nava-Saucedo, J.-E. Polymer biodegradation: Mechanisms and estimation techniques-A review. *Chemosphere* **2008,** *73*(4), 429-442.
[9] Mahajan, N.; Gupta, P. New insights into the microbial degradation of polyurethanes. *RSC Adv.* **2015,** *5*(52), 41839-41854.
[10] Ignatyev, I. A.; Thielemans, W.; Vander Beke, B. Recycling of polymers: A review. *ChemSusChem.* **2014,** *7*(6), 1579-1593.
[11] Sarkhel, R.; Sengupta, S.; Das, P.; Bhowal, A. Comparative biodegradation study of polymer from plastic bottle waste using novel isolated bacteria and fungi from marine source. *J. Polym. Res*. **2020,** *27*, 1-8.
[12] Zhang, J.; Gao, D.; Li, Q.; Zhao, Y.; Li, L.; Lin, H.; Bi, Q.; Zhao, Y. Biodegradation of polyethylene microplastic particles by the fungus Aspergillus flavus from the guts of wax moth Galleria mellonella. *Sci. Total Environ.* **2020,** *704*, 135931.
[13] Karunarathna, B.; Wanniarachchi, J. D.; Prashantha, M.; Govender, K. Enhancing styrene monomer recovery from polystyrene pyrolysis: insights from density functional theory. *J. Mol. Model.* **2023,** *29*(8), 255.
[14] Cregut, M.; Bedas, M.; Durand, M.-J.; Thouand, G. New insights into polyurethane biodegradation and realistic prospects for the development of a sustainable waste recycling process. *Biotechnol. Adv.* **2013,** *31*(8), 1634-1647.
[15] Falkiewicz-Dulik, M.; Janda, K.; Wypych, G. *Handbook of material biodegradation, biodeterioration, and biostablization*; Elsevier, 2015.
[16] Li, S.; Wang, J.; Tuo, X.; He, Y. Hydrophilization of polyurethane foam carriers in MBBR with hyperbranched polymeric diazonium salts. *Chem. Res. Chin. Univ.* **2018,** *34*, 844-848.
[17] Mukherjee, K.; Tribedi, P.; Chowdhury, A.; Ray, T.; Joardar, A.; Giri, S.; Sil, A. K. Isolation of a Pseudomonas aeruginosa strain from soil that can degrade polyurethane diol. *Biodegradation* **2011,** *22*, 377-388.
[18] Howard, G. T.; Norton, W. N.; Burks, T. Growth of Acinetobacter gerneri P7 on polyurethane and the purification and characterization of a polyurethanase enzyme. *Biodegradation* **2012,** *23*, 561-573.
[19] Peng, Y. H.; Shih, Y. H.; Lai, Y. C.; Liu, Y. Z.; Liu, Y. T.; Lin, N. C. Degradation of polyurethane by bacterium isolated from soil and assessment of polyurethanolytic activity of a Pseudomonas putida strain. *Environ Sci Pollut Res Int.* **2014,** *21*(16), 9529-9537.
[20] Magnin, A.; Pollet, E.; Phalip, V.; Avérous, L. Evaluation of biological degradation of polyurethanes. *Biotechnol. Adv.* **2020,** *39*, 107457.
[21] Bhandari, S.; Poudel, D. K.; Marahatha, R.; Dawadi, S.; Khadayat, K.; Phuyal, S.; Shrestha, S.; Gaire, S.; Basnet, K.; Khadka, U. Microbial enzymes used in bioremediation. *J. Chem.* **2021,** *2021*(1), 8849512.
[22] Beneš, H.; Vlčková, V.; Paruzel, A.; Trhlíková, O.; Chalupa, J.; Kanizsová, L.; Skleničková, K.; Halecký, M. Multifunctional and fully aliphatic biodegradable polyurethane foam as porous biomass carrier for biofiltration. *Polym. Degrad. Stab*. **2020,** *176*, 109156.
[23] Biffinger, J. C.; Barlow, D. E.; Cockrell, A. L.; Cusick, K. D.; Hervey, W. J.; Fitzgerald, L. A.; Nadeau, L. J.; Hung, C. S.; Crookes-Goodson, W. J.; Russell Jr, J. N. The applicability of Impranil® DLN for gauging the biodegradation of polyurethanes. *Polym. Degrad. Stab*. **2015,** *120*, 178-185.
[24] Ruiz, C.; Main, T.; Hilliard, N. P.; Howard, G. T. Purification and characterization of twopolyurethanase enzymes from Pseudomonas chlororaphis. *Int Biodeter Biodegr.* **1999,** *43*(1-2), 43-47.
[25] Chen, H.; Hui, W.; Aijun, Z.; Zuohu, L. Alkaline protease production by solid state fermentation on polyurethane foam. *Chem. Biochem. Eng. Q*. **2006,** *20*(1), 93-97.
[26] Howard, G. T.; Blake, R. C. Growth of Pseudomonas fluorescens on a polyester-polyurethane and the purification and characterization of a polyurethanase-protease enzyme. *Int Biodeter Biodegr.* **1998,** *42*(4), 213-220.
[27] Wang, H.; Fu, Y.; Liu, R.; Xiong, J.; Li, N. Waterproof, breathable and infrared-invisible polyurethane/silica nanofiber membranes for wearable textiles. *J. Chem. Soc. Dalton Trans*. **2022,** *51*(36), 13949-13956.
[28] Ma, J.; Lee, G.-H.; Kim, J.-H.; Kim, S.-W.; Jo, S.; Kim, C. S. A transparent self-healing polyurethane-isophorone-

diisocyanate elastomer based on hydrogen-bonding interactions. *ACS Appl. Polym. Mater*. **2022,** *4*(4), 2497-2505.
[29] Coudert, E.; Gehant, S.; de Castro, E.; Pozzato, M.; Baratin, D.; Neto, T.; Sigrist, C. J.; Redaschi, N.; Bridge, A. Annotation of biologically relevant ligands in UniProtKB using ChEBI. *Bioinformatics* **2023,** *39*(1), btac793.
[30] Zhou, X.; Zheng, W.; Li, Y.; Pearce, R.; Zhang, C.; Bell, E. W.; Zhang, G.; Zhang, Y. I-TASSER-MTD: A deep-learning-based platform for multi-domain protein structure and function prediction. *Nat. Protoc*. **2022,** *17*(10), 2326-2353.
[31] Olsson, M. H.; Søndergaard, C. R.; Rostkowski, M.; Jensen, J. H. PROPKA3: Consistent treatment of internal and surface residues in empirical pK_a predictions. *J. Chem. Theory Comput*. **2011,** *7*(2), 525-537.
[32] Abd Rahman, R. N. Z.; Geok, L. P.; Basri, M.; Salleh, A. B. Physical factors affecting the production of organic solvent-tolerant protease by Pseudomonas aeruginosa strain K. *Bioresour. Technol*. **2005,** *96*(4), 429-436.
[33] Phillips, J. C.; Hardy, D. J.; Maia, J. D.; Stone, J. E.; Ribeiro, J. V.; Bernardi, R. C.; Buch, R.; Fiorin, G.; Hénin, J.; Jiang, W. Scalable molecular dynamics on CPU and GPU architectures with NAMD. *J. Chem. Phys*. **2020,** *153*(4), 044130.
[34] Jo, S.; Kim, T.; Iyer, V. G.; Im, W. CHARMM-GUI: A web-based graphical user interface for CHARMM. *J. Comput. Chem*. **2008,** *29*(11), 1859-1865.
[35] Haug, E.; Arora, J.; Matsui, K. A steepest-descent method for optimization of mechanical systems. *J. Optim. Theory Appl*. **1976,** *19*, 401-424.
[36] Akram, S.; Ann, Q. U. Newton raphson method. *Int. J. Sci. Eng. Res*. **2015,** *6*(7), 1748-1752.
[37] Darden, T.; York, D.; Pedersen, L. Particle mesh Ewald: An $N\cdot\log(N)$ method for Ewald sums in large systems. *J. Chem. Phys*. **1993,** *98*(12), 10089-10092.
[38] Laskowski, R.; MacArthur, M.; Thornton, J. PROCHECK: Validation of protein-structure coordinates. *Int. Tables Crystallogr*. **2006,** *F*, 722-725.
[39] Wiederstein, M.; Sippl, M. J. ProSA-web: Interactive web service for the recognition of errors in three-dimensional structures of proteins. *Nucleic Acids Res.* **2007,** *35*(suppl_2), W407-W410.
[40] Colovos, C.; Yeates, T. O. Verification of protein structures: patterns of nonbonded atomic interactions. *Prot. Sci.* **1993,** *2*(9), 1511-1519.
[41] Bowie, J. U.; Lüthy, R.; Eisenberg, D. A method to identify protein sequences that fold into a known three-dimensional structure. *Science* **1991,** *253*(5016), 164-170.
[42] Jurcik, A.; Bednar, D.; Byska, J.; Marques, S. M.; Furmanova, K.; Daniel, L.; Kokkonen, P.; Brezovsky, J.; Strnad, O.; Stourac, J. CAVER Analyst 2.0: Analysis and visualization of channels and tunnels in protein structures and molecular dynamics trajectories. *Bioinformatics* **2018,** *34*(20), 3586-3588.
[43] Pavelka, A.; Sebestova, E.; Kozlikova, B.; Brezovsky, J.; Sochor, J.; Damborsky, J. CAVER: Algorithms for analyzing dynamics of tunnels in macromolecules. *IEEE/ACM Trans. Comput. Biol. Bioinform*. **2015,** *13*(3), 505-517.
[44] Dennington, R.; Keith, T. A.; Millam, J. M. *GaussView, version 6.0. 16*; Semichem Inc., Shawnee Mission, KS, USA, 2016.
[45] Rassolov, V. A.; Ratner, M. A.; Pople, J. A.; Redfern, P. C.; Curtiss, L. A. 6-31G* basis set for third-row atoms. *J. Comput. Chem*. **2001,** *22*(9), 976-984.
[46] Caricato, M.; Frisch, M. J.; Hiscocks, J.; Frisch, M. J. *Gaussian 09: IOps Reference*; Gaussian Wallingford, CT, USA, 2009.
[47] Morris, G. M.; Huey, R.; Lindstrom, W.; Sanner, M. F.; Belew, R. K.; Goodsell, D. S.; Olson, A. J. AutoDock4 and AutoDockTools4: Automated docking with selective receptor flexibility. *J. Comput. Chem*. **2009,** *30*(16), 2785-2791.
[48] Morris, G. M.; Goodsell, D. S.; Halliday, R. S.; Huey, R.; Hart, W. E.; Belew, R. K.; Olson, A. J. Automated docking using a Lamarckian genetic algorithm and an empirical binding free energy function. *J. Comput. Chem*. **1988,** *19*(14), 1639-1662.
[49] Gangadharan, R.; Sampath Krishnan, S. Natural Bond Orbital (NBO) population analysis of 1-azanapthalene-8-ol. *Acta Phys. Pol. A*. **2014,** *125*(1), 18-22.
[50] Sánchez-Márquez, J.; Zorrilla, D.; Sánchez-Coronilla, A.; de los Santos, D. M.; Navas, J.; Fernández-Lorenzo, C.; Alcántara, R.; Martín-Calleja, J. Introducing "UCA-FUKUI" software: Reactivity-index calculations. *J. Mol. Model*. **2014,** *20*, 1-13.
[51] Cerón, M. L.; Calatayud, M. Application of dual descriptor to understand the activity of Cu/ZrO_2 catalysts in the water gas shift reaction. *J. Mol. Model*. **2017,** *23*, 1-8.
[52] Huang, J.; MacKerell Jr, A. D. CHARMM36 all-atom additive protein force field: Validation based on comparison to NMR data. *J. Comput. Chem*. **2013,** *34*(25), 2135-2145.

[53] Metropolis, N.; Ulam, S. The monte carlo method. *J. Am. Stat. Assoc*. **1949,** *44*(247), 335-341.
[54] Humphrey, W.; Dalke, A.; Schulten, K. VMD: Visual molecular dynamics. *J. Mol. Graph*. **1996,** *14*(1), 33-38.
[55] Kumari, R.; Kumar, R.; Consortium, O. S. D. D.; Lynn, A. *g_mmpbsa*-A GROMACS tool for high-throughput MM-PBSA calculations. *J. Chem. Inf. Model*. **2014,** *54*(7), 1951-1962.
[56] Karunarathna, B.; Jayakody, R. S.; Karunanayake, L.; Govender, K. K. Computational development and validation of a representative MDI-BDO-based polyurethane hard segment model. *J. Mol. Model*. **2021,** *27*, 1-20.
[57] Krieger, E.; Nabuurs, S. B.; Vriend, G. Homology modeling. *Struct. Bioinform.* **2003,** *44*, 509-523.
[58] Barcellos, G. B.; Pauli, I.; Caceres, R. A.; Macedo, L. F. S. Molecular modeling as a tool for drug discovery. *Curr. Drug Targets*. **2008,** *9*, 1084-1091.
[59] Yang, J.; Roy, A.; Zhang, Y. Protein-ligand binding site recognition using complementary binding-specific substructure comparison and sequence profile alignment. *Bioinformatics* **2013,** *29*(20), 2588-2595.
[60] Vanommeslaeghe, K.; Hatcher, E.; Acharya, C.; Kundu, S.; Zhong, S.; Shim, J.; Darian, E.; Guvench, O.; Lopes, P.; Vorobyov, I. CHARMM general force field: A force field for drug-like molecules compatible with the CHARMM all-atom additive biological force fields. *J. Comput. Chem*. **2010,** *31*(4), 671-690.
[61] Laskowski, R. A.; MacArthur, M. W.; Moss, D. S.; Thornton, J. M. PROCHECK: A program to check the stereochemical quality of protein structures. *J. Appl. Crystallogr*. **1993,** *26*(2), 283-291.
[62] Wlodawer, A.; Li, M.; Dauter, Z.; Gustchina, A.; Uchida, K.; Oyama, H.; Dunn, B. M.; Oda, K. Carboxyl proteinase from Pseudomonas defines a novel family of subtilisin-like enzymes. *Nat. Struct. Mol. Biol*. **2001,** *8*(5), 442-446.
[63] Kawabata, T. Detection of multiscale pockets on protein surfaces using mathematical morphology. *Proteins: Struct. Funct. Bioinf*. **2010,** *78*(5), 1195-1211.
[64] Design, L. Pharmacophore and ligand-based design with Biovia Discovery Studio®. *BIOVIA. California* **2014**.
[65] Melin, J.; Aparicio, F.; Subramanian, V.; Galván, M.; Chattaraj, P. K. Is the fukui function a right descriptor of hard-hard interactions? *J. Phys. Chem. A*. **2004,** *108*(13), 2487-2491.
[66] Martínez-Araya, J. I. Why is the dual descriptor a more accurate local reactivity descriptor than Fukui functions? *J. Math. Chem*. **2015,** *53*(2), 451-465.

Appendix 1. Computational studies of biodegradation of polyester-polyurethanes by protease enzyme

Table A1. Optimized structure parameters of PU-HDI (degrees and Angstroms)

Definition	Value	Definition	Value	Definition	Value	Definition	Value
R (1, 2)	1.3656	A (2, 1, 4)	116.7994	A (71, 70, 72)	124.2988	D (48, 50, 53, 54)	-57.1495
R (1, 4)	1.4439	A (1, 2, 3)	125.1101	A (70, 72, 73)	114.4906	D (48, 50, 53, 55)	58.7914
R (2, 3)	1.2193	A (1, 2, 48)	109.5504	A (72, 73, 74)	110.9379	D (48, 50, 53, 56)	-179.3617
R (2, 48)	1.3622	A (3, 2, 48)	125.3345	A (72, 73, 75)	105.578	D (51, 50, 53, 54)	64.6235
R (4, 5)	1.5241	A (1, 4, 5)	111.0444	A (72, 73, 76)	110.9167	D (51, 50, 53, 55)	-179.4356
R (4, 15)	1.0942	A (1, 4, 15)	105.7177	A (74, 73, 75)	110.385	D (51, 50, 53, 56)	-57.5887
R (4, 16)	1.0923	A (1, 4, 16)	108.6211	A (74, 73, 76)	108.6893	D (52, 50, 53, 54)	-176.9605
R (5, 6)	1.5336	A (5, 4, 15)	110.5618	A (75, 73, 76)	110.322	D (52, 50, 53, 55)	-61.0196
R (5, 17)	1.098	A (5, 4, 16)	111.4224	D (4, 1, 2, 3)	-1.7393	D (52, 50, 53, 56)	60.8273
R (5, 18)	1.0965	A (15, 4, 16)	109.2898	D (4, 1, 2, 48)	177.489	D (50, 53, 56, 57)	-57.8238
R (6, 7)	1.5198	A (4, 5, 6)	113.8663	D (2, 1, 4, 5)	109.0897	D (50, 53, 56, 58)	57.9414
R (6, 19)	1.0959	A (4, 5, 17)	109.1744	D (2, 1, 4, 15)	-130.9624	D (50, 53, 56, 59)	-179.8736
R (6, 20)	1.0964	A (4, 5, 18)	107.6557	D (2, 1, 4, 16)	-13.7713	D (54, 53, 56, 57)	-179.816
R (7, 8)	1.4476	A (6, 5, 17)	109.7656	D (1, 2, 48, 49)	7.0752	D (54, 53, 56, 58)	-64.0508
R (7, 21)	1.0944	A (6, 5, 18)	109.4047	D (1, 2, 48, 50)	172.983	D (54, 53, 56, 59)	58.1341
R (7, 22)	1.0955	A (17, 5, 18)	106.7114	D (3, 2, 48, 49)	-173.6987	D (55, 53, 56, 57)	63.1431
R (8, 9)	1.3528	A (5, 6, 7)	113.3962	D (3, 2, 48, 50)	-7.7909	D (55, 53, 56, 58)	178.9083
R (9, 10)	1.2125	A (5, 6, 19)	110.0415	D (1, 4, 5, 6)	-65.0178	D (55, 53, 56, 59)	-58.9068
R (9, 14)	1.5161	A (5, 6, 20)	109.7297	D (1, 4, 5, 17)	58.0317	D (53, 56, 59, 60)	-57.6045
R (11, 12)	1.5291	A (7, 6, 19)	109.4662	D (1, 4, 5, 18)	173.5100	D (53, 56, 59, 61)	57.9970
R (11, 29)	1.0974	A (7, 6, 20)	107.4733	D (15, 4, 5, 6)	177.9601	D (53, 56, 59, 62)	-179.9284
R (11, 30)	1.0977	A (19, 6, 20)	106.473	D (15, 4, 5, 17)	-58.9904	D (57, 56, 59, 60)	-179.7011
R (11, 31)	1.5164	A (6, 7, 8)	107.9997	D (15, 4, 5, 18)	56.4880	D (57, 56, 59, 61)	-64.0996
R (12, 13)	1.532	A (6, 7, 21)	111.6935	D (16, 4, 5, 6)	56.2122	D (57, 56, 59, 62)	57.9750
R (12, 27)	1.0966	A (6, 7, 22)	112.0049	D (16, 4, 5, 17)	179.2617	D (58, 56, 59, 60)	64.6969
R (12, 28)	1.0965	A (8, 7, 21)	108.7736	D (16, 4, 5, 18)	-65.2599	D (58, 56, 59, 61)	-179.7017
R (13, 14)	1.5291	A (8, 7, 22)	108.7688	D (4, 5, 6, 7)	-177.7031	D (58, 56, 59, 62)	-57.6271
R (13, 25)	1.0965	A (21, 7, 22)	107.5251	D (4, 5, 6, 19)	-54.7234	D (56, 59, 62, 63)	-58.9186
R (13, 26)	1.0966	A (7, 8, 9)	116.0369	D (4, 5, 6, 20)	62.1162	D (56, 59, 62, 64)	58.1373
R (14, 23)	1.0974	A (8, 9, 10)	123.5026	D (17, 5, 6, 7)	59.5707	D (56, 59, 62, 65)	-179.8704
R (14, 24)	1.0977	A (8, 9, 14)	110.8853	D (17, 5, 6, 19)	-177.4497	D (60, 59, 62, 63)	178.8887
R (31, 32)	1.2129	A (10, 9, 14)	125.6121	D (17, 5, 6, 20)	-60.6101	D (60, 59, 62, 64)	-64.0554
R (31, 33)	1.3516	A (12, 11, 29)	111.2898	D (18, 5, 6, 7)	-57.2073	D (60, 59, 62, 65)	57.9369
R (33, 34)	1.446	A (12, 11, 30)	111.1786	D (18, 5, 6, 19)	65.7724	D (61, 59, 62, 63)	63.1154
R (34, 35)	1.0956	A (12, 11, 31)	113.0675	D (18, 5, 6, 20)	-177.388	D (61, 59, 62, 64)	-179.8288
R (34, 36)	1.0954	A (29, 11, 30)	105.3262	D (5, 6, 7, 8)	63.4556	D (61, 59, 62, 65)	-57.8365
R (34, 37)	1.5196	A (29, 11, 31)	107.8776	D (5, 6, 7, 21)	-176.9774	D (59, 62, 65, 66)	-57.7064
R (37, 38)	1.0941	A (30, 11, 31)	107.7204	D (5, 6, 7, 22)	-56.2930	D (59, 62, 65, 67)	60.6975
R (37, 39)	1.0976	A (11, 12, 13)	112.4653	D (19, 6, 7, 8)	-59.8405	D (59, 62, 65, 68)	-179.5404
R (37, 40)	1.5336	A (11, 12, 27)	109.0757	D (19, 6, 7, 21)	59.7265	D (63, 62, 65, 66)	-179.5613
R (40, 41)	1.0975	A (11, 12, 28)	109.0399	D (19, 6, 7, 22)	-179.5891	D (63, 62, 65, 67)	-61.1573
R (40, 42)	1.098	A (13, 12, 27)	110.1633	D (20, 6, 7, 8)	-175.0904	D (63, 62, 65, 68)	58.6047
R (40, 43)	1.524	A (13, 12, 28)	110.2014	D (20, 6, 7, 21)	-55.5234	D (64, 62, 65, 66)	64.5028
R (43, 44)	1.1015	A (27, 12, 28)	105.6587	D (20, 6, 7, 22)	65.1610	D (64, 62, 65, 67)	-177.0933
R (43, 45)	1.1026	A (12, 13, 14)	112.4415	D (6, 7, 8, 9)	-178.4452	D (64, 62, 65, 68)	-57.3312
R (43, 46)	1.4241	A (12, 13, 25)	110.1884	D (21, 7, 8, 9)	60.1591	D (62, 65, 68, 69)	75.0000
R (46, 47)	0.9651	A (12, 13, 26)	110.1898	D (22, 7, 8, 9)	-56.6755	D (62, 65, 68, 70)	-87.7196
R (48, 49)	1.009	A (14, 13, 25)	109.0644	D (7, 8, 9, 10)	0.06450	D (66, 65, 68, 69)	-48.0261
R (48, 50)	1.455	A (14, 13, 26)	109.0529	D (7, 8, 9, 14)	-179.9261	D (66, 65, 68, 70)	149.2542
R (50, 51)	1.0965	A (25, 13, 26)	105.6693	D (8, 9, 14, 13)	179.2964	D (67, 65, 68, 69)	-163.4849
R (50, 52)	1.0929	A (9, 14, 13)	113.0946	D (8, 9, 14, 23)	55.8644	D (67, 65, 68, 70)	33.7954
R (50, 53)	1.5347	A (9, 14, 23)	107.8088	D (8, 9, 14, 24)	-57.3817	D (65, 68, 70, 71)	-8.8115
R (53, 54)	1.0991	A (9, 14, 24)	107.7935	D (10, 9, 14, 13)	-124.126	D (65, 68, 70, 72)	172.2168
R (53, 55)	1.097	A (13, 14, 23)	111.2564	D (10, 9, 14, 23)	122.6279	D (69, 68, 70, 71)	-171.9956
R (53, 56)	1.5331	A (13, 14, 24)	111.1787	D (10, 9, 14, 24)	-58.7818	D (69, 68, 70, 72)	9.0327
R (56, 57)	1.0986	A (23, 14, 24)	105.3273	D (29, 11, 12, 13)	63.7433	D (68, 70, 72, 73)	178.369
R (56, 58)	1.0996	A (11, 31, 32)	125.5296	D (29, 11, 12, 27)	178.6699	D (71, 70, 72, 73)	-0.6209
R (56, 59)	1.5338	A (11, 31, 33)	110.8558	D (29, 11, 12, 28)	58.2959	D (70, 72, 73, 74)	59.7425
R (59, 60)	1.0997	A (32, 31, 33)	123.6145	D (30, 11, 12, 13)	-179.179	D (70, 72, 73, 75)	179.3362
R (59, 61)	1.0987	A (31, 33, 34)	115.9807	D (30, 11, 12, 27)	-64.2523	D (70, 72, 73, 76)	-61.1568
R (59, 62)	1.5331	A (33, 34, 35)	108.8796	D (30, 11, 12, 28)	179.6137		
R (62, 63)	1.0968	A (33, 34, 36)	108.9569	D (31, 11, 12, 13)	-57.8612		
R (62, 64)	1.0991	A (33, 34, 37)	107.6977	D (31, 11, 12, 27)	57.0655		

Table A1. (cont.)

Definition	Value	Definition	Value	Definition	Value	Definition	Value
R (62, 65)	1.5348	A (35, 34, 36)	107.3097	D (31, 11, 12, 28)	-1.5099		
R (65, 66)	1.0965	A (35, 34, 37)	112.0793	D (12, 11, 31, 32)	178.5827		
R (65, 67)	1.0931	A (36, 34, 37)	111.8531	D (12, 11, 31, 33)	-125.0161		
R (65, 68)	1.4549	A (34, 37, 38)	109.5844	D (29, 11, 31, 32)	55.0765		
R (68, 69)	1.0091	A (34, 37, 39)	109.0121	D (29, 11, 31, 33)	121.7412		
R (68, 70)	1.3636	A (34, 37, 40)	111.9521	D (30, 11, 31, 32)	-58.1661		
R (70, 71)	1.2184	A (38, 37, 39)	106.9413	D (30, 11, 31, 33)	179.897		
R (70, 72)	1.3634	A (38, 37, 40)	109.3698	D (11, 12, 13, 14)	-58.206		
R (72, 73)	1.4328	A (39, 37, 40)	109.8515	D (11, 12, 13, 25)	58.0138		
R (73, 74)	1.093	A (37, 40, 41)	109.9688	D (11, 12, 13, 26)	57.9872		
R (73, 75)	1.0904	A (37, 40, 42)	110.2888	D (27, 12, 13, 14)	179.8841		
R (73, 76)	1.093	A (37, 40, 43)	113.0541	D (27, 12, 13, 25)	-63.896		
		A (41, 40, 42)	106.8112	D (27, 12, 13, 26)	-58.2118		
		A (41, 40, 43)	108.2017	D (28, 12, 13, 14)	63.6852		
		A (42, 40, 43)	108.2963	D (28, 12, 13, 25)	179.9050		
		A (40, 43, 44)	109.4517	D (28, 12, 13, 26)	179.7620		
		A (40, 43, 45)	109.6263	D (12, 13, 14, 9)	-58.7284		
		A (40, 43, 46)	108.156	D (12, 13, 14, 23)	58.3296		
		A (44, 43, 45)	107.3489	D (12, 13, 14, 24)	57.2289		
		A (44, 43, 46)	111.1101	D (25, 13, 14, 9)	178.7385		
		A (45, 43, 46)	111.1355	D (25, 13, 14, 23)	-64.2035		
		A (43, 46, 47)	108.1916	D (25, 13, 14, 24)	-57.7113		
		A (2, 48, 49)	116.8813	D (26, 13, 14, 9)	63.7983		
		A (2, 48, 50)	121.7314	D (26, 13, 14, 23)	-179.1437		
		A (49, 48, 50)	119.8672	D (26, 13, 14, 24)	179.7091		
		A (48, 50, 51)	108.1487	D (11, 31, 33, 34)	-0.2004		
		A (48, 50, 52)	106.8131	D (32, 31, 33, 34)	58.0712		
		A (48, 50, 53)	113.8562	D (31, 33, 34, 35)	-58.6693		
		A (51, 50, 52)	107.5272	D (31, 33, 34, 36)	179.815		
		A (51, 50, 53)	110.2851	D (31, 33, 34, 37)	58.8088		
		A (52, 50, 53)	109.9646	D (33, 34, 37, 38)	-57.9167		
		A (50, 53, 54)	109.3156	D (33, 34, 37, 39)	-179.6612		
		A (50, 53, 55)	108.3865	D (33, 34, 37, 40)	178.5427		
		A (50, 53, 56)	112.6151	D (35, 34, 37, 38)	61.8172		
		A (54, 53, 55)	106.7031	D (35, 34, 37, 39)	-59.9272		
		A (54, 53, 56)	109.705	D (35, 34, 37, 40)	-60.8852		
		A (55, 53, 56)	109.9331	D (36, 34, 37, 38)	-177.6107		
		A (53, 56, 57)	109.2957	D (36, 34, 37, 39)	60.6448		
		A (53, 56, 58)	109.4427	D (36, 34, 37, 40)	-56.8897		
		A (53, 56, 59)	113.3269	D (34, 37, 40, 41)	60.6524		
		A (57, 56, 58)	106.074	D (34, 37, 40, 42)	-177.9427		
		A (57, 56, 59)	109.2118	D (34, 37, 40, 43)	64.7637		
		A (58, 56, 59)	109.2334	D (38, 37, 40, 41)	-177.6942		
		A (56, 59, 60)	109.2307	D (38, 37, 40, 42)	-56.2893		
		A (56, 59, 61)	109.211	D (38, 37, 40, 43)	-178.151		
		A (56, 59, 62)	113.3177	D (39, 37, 40, 41)	-60.6088		
		A (60, 59, 61)	106.0752	D (39, 37, 40, 42)	60.7961		
		A (60, 59, 62)	109.4666	D (39, 37, 40, 43)	-176.0037		
		A (61, 59, 62)	109.2839	D (37, 40, 43, 44)	-58.5078		
		A (59, 62, 63)	109.951	D (37, 40, 43, 45)	62.812		
		A (59, 62, 64)	109.7011	D (37, 40, 43, 46)	61.9476		
		A (59, 62, 65)	112.6162	D (41, 40, 43, 44)	179.4435		
		A (63, 62, 64)	106.7086	D (41, 40, 43, 45)	-59.2367		
		A (63, 62, 65)	108.3643	D (41, 40, 43, 46)	-53.4809		
		A (64, 62, 65)	109.3171	D (42, 40, 43, 44)	64.015		
		A (62, 65, 66)	110.3183	D (42, 40, 43, 45)	-174.6652		
		A (62, 65, 67)	109.9091	D (42, 40, 43, 46)	-176.0021		
		A (62, 65, 68)	113.9096	D (40, 43, 46, 47)	63.8471		
		A (66, 65, 67)	107.5286	D (44, 43, 46, 47)	-55.6211		
		A (66, 65, 68)	108.1473	D (45, 43, 46, 47)	147.7016		
		A (67, 65, 68)	106.7781	D (2, 48, 50, 51)	32.2261		
		A (65, 68, 69)	119.6414	D (2, 48, 50, 52)	-89.3501		
		A (65, 68, 70)	121.3657	D (2, 48, 50, 53)	-46.8018		
		A (69, 68, 70)	116.821	D (49, 48, 50, 51)	-162.2773		
		A (68, 70, 71)	125.7506	D (49, 48, 50, 52)	76.1465		
		A (68, 70, 72)	109.9421	D (49, 48, 50, 53)			

Table A2. Optimized structure parameters of PU-IPDI (degrees and Angstroms)

Definition	Value	Definition	Value	Definition	Value	Definition	Value
R (1, 2)	1.3669	A (2, 1, 4)	116.8086	A (75, 74, 76)	107.8364	D (50, 52, 54, 55)	179.5641
R (1, 4)	1.4429	A (1, 2, 3)	124.8904	A (75, 74, 77)	107.8208	D (53, 52, 54, 55)	-0.4147
R (2, 3)	1.2204	A (1, 2, 48)	109.5598	A (76, 74, 77)	107.6398	D (52, 54, 55, 56)	60.8317
R (2, 48)	1.3596	A (3, 2, 48)	125.5476	A (64, 78, 79)	110.8111	D (52, 54, 55, 57)	-179.6346
R (4, 5)	1.5244	A (1, 4, 5)	111.0994	A (64, 78, 80)	110.0368	D (52, 54, 55, 58)	-60.1073
R (4, 15)	1.0943	A (1, 4, 15)	105.7213	A (64, 78, 81)	113.484	D (64, 59, 60, 48)	-179.9087
R (4, 16)	1.0924	A (1, 4, 16)	108.6617	A (79, 78, 80)	107.6266	D (64, 59, 60, 61)	-57.47600
R (5, 6)	1.5336	A (5, 4, 15)	110.5097	A (79, 78, 81)	107.6698	D (64, 59, 60, 82)	64.4022
R (5, 17)	1.0980	A (5, 4, 16)	111.3787	A (80, 78, 81)	106.969	D (66, 59, 60, 48)	-58.8702
R (5, 18)	1.0966	A (15, 4, 16)	109.2900	A (62, 83, 84)	110.2928	D (66, 59, 60, 61)	63.5625
R (6, 7)	1.5198	A (4, 5, 6)	113.859	A (62, 83, 85)	111.0556	D (66, 59, 60, 82)	-174.5593
R (6, 19)	1.0959	A (4, 5, 17)	109.1595	A (62, 83, 86)	112.9753	D (67, 59, 60, 48)	56.9417
R (6, 20)	1.0963	A (4, 5, 18)	107.6688	A (84, 83, 85)	108.0946	D (67, 59, 60, 61)	179.3744
R (7, 8)	1.4479	A (6, 5, 17)	109.7524	A (84, 83, 86)	106.7119	D (67, 59, 60, 82)	-58.7474
R (7, 21)	1.0944	A (6, 5, 18)	109.4149	A (85, 83, 86)	107.4871	D (60, 59, 64, 63)	50.7757
R (7, 22)	1.0955	A (17, 5, 18)	106.7254	D (4, 1, 2, 3)	-1.7216	D (60, 59, 64, 74)	168.2545
R (8, 9)	1.3524	A (5, 6, 7)	113.413	D (4, 1, 2, 48)	177.768	D (60, 59, 64, 78)	-74.0718
R (9, 10)	1.2126	A (5, 6, 19)	110.0413	D (2, 1, 4, 5)	108.6059	D (66, 59, 64, 63)	-69.6825
R (9, 14)	1.5162	A (5, 6, 20)	109.7162	D (2, 1, 4, 15)	-131.4767	D (66, 59, 64, 74)	47.7963
R (11, 12)	1.5291	A (7, 6, 19)	109.4758	D (2, 1, 4, 16)	-14.2635	D (66, 59, 64, 78)	165.4700
R (11, 29)	1.0974	A (7, 6, 20)	107.4687	D (1, 2, 48, 49)	4.1454	D (67, 59, 64, 63)	173.559
R (11, 30)	1.0976	A (19, 6, 20)	106.4632	D (1, 2, 48, 60)	175.4135	D (67, 59, 64, 74)	-68.9622
R (11, 31)	1.5164	A (6, 7, 8)	108.0155	D (3, 2, 48, 49)	-176.3692	D (67, 59, 64, 78)	48.7115
R (12, 13)	1.5320	A (6, 7, 21)	111.7147	D (3, 2, 48, 60)	-5.1011	D (48, 60, 61, 62)	-179.6747
R (12, 27)	1.0966	A (6, 7, 22)	112.0035	D (1, 4, 5, 6)	-64.9999	D (48, 60, 61, 65)	-56.5342
R (12, 28)	1.0965	A (8, 7, 21)	108.7607	D (1, 4, 5, 17)	58.0161	D (48, 60, 61, 70)	59.1629
R (13, 14)	1.5291	A (8, 7, 22)	108.7441	D (1, 4, 5, 18)	173.5102	D (59, 60, 61, 62)	56.7608
R (13, 25)	1.0965	A (21, 7, 22)	107.5253	D (15, 4, 5, 6)	177.9721	D (59, 60, 61, 65)	179.9013
R (13, 26)	1.0966	A (7, 8, 9)	116.0609	D (15, 4, 5, 17)	-59.0119	D (59, 60, 61, 70)	-64.4016
R (14, 23)	1.0975	A (8, 9, 10)	123.5339	D (15, 4, 5, 18)	56.4823	D (82, 60, 61, 62)	-64.5778
R (14, 24)	1.0976	A (8, 9, 14)	110.8821	D (16, 4, 5, 6)	56.2898	D (82, 60, 61, 65)	58.5626
R (31, 32)	1.2129	A (10, 9, 14)	125.5839	D (16, 4, 5, 17)	179.3058	D (82, 60, 61, 70)	174.2598
R (31, 33)	1.3516	A (12, 11, 29)	111.2659	D (16, 4, 5, 18)	-65.2000	D (60, 61, 62, 63)	-49.9385
R (33, 34)	1.4460	A (12, 11, 30)	111.2007	D (4, 5, 6, 7)	-177.6342	D (60, 61, 62, 71)	-165.5285
R (34, 35)	1.0957	A (12, 11, 31)	113.0733	D (4, 5, 6, 19)	-54.6303	D (60, 61, 62, 83)	75.4056
R (34, 36)	1.0954	A (29, 11, 30)	105.3238	D (4, 5, 6, 20)	62.1892	D (65, 61, 62, 63)	-172.7952
R (34, 37)	1.5196	A (29, 11, 31)	107.8477	D (17, 5, 6, 7)	59.6741	D (65, 61, 62, 71)	71.6147
R (37, 38)	1.0941	A (30, 11, 31)	107.7482	D (17, 5, 6, 19)	-177.3219	D (65, 61, 62, 83)	-47.4512
R (37, 39)	1.0976	A (11, 12, 13)	112.4658	D (17, 5, 6, 20)	-60.5025	D (70, 61, 62, 63)	71.1476
R (37, 40)	1.5336	A (11, 12, 27)	109.0749	D (18, 5, 6, 7)	-57.1191	D (70, 61, 62, 71)	-44.4425
R (40, 41)	1.0975	A (11, 12, 28)	109.0396	D (18, 5, 6, 19)	65.8849	D (70, 61, 62, 83)	-163.5084
R (40, 42)	1.0980	A (13, 12, 27)	110.1757	D (18, 5, 6, 20)	-177.2957	D (61, 62, 63, 64)	46.4807
R (40, 43)	1.5240	A (13, 12, 28)	110.1907	D (5, 6, 7, 8)	63.4250	D (61, 62, 63, 68)	172.2984
R (43, 44)	1.1015	A (27, 12, 28)	105.6576	D (5, 6, 7, 21)	-177.001	D (61, 62, 63, 69)	-73.6182
R (43, 45)	1.1026	A (12, 13, 14)	112.4511	D (5, 6, 7, 22)	-56.3024	D (71, 62, 63, 64)	164.2582
R (43, 46)	1.4241	A (12, 13, 25)	110.1843	D (19, 6, 7, 8)	-59.8898	D (71, 62, 63, 68)	-69.9241
R (46, 47)	0.9651	A (12, 13, 26)	110.1924	D (19, 6, 7, 21)	59.6841	D (71, 62, 63, 69)	44.1593
R (48, 49)	1.0099	A (14, 13, 25)	109.0582	D (19, 6, 7, 22)	-179.6173	D (83, 62, 63, 64)	-77.6172
R (48, 60)	1.4599	A (14, 13, 26)	109.0551	D (20, 6, 7, 8)	-175.1306	D (83, 62, 63, 68)	48.2005
R (50, 51)	1.0079	A (25, 13, 26)	105.6644	D (20, 6, 7, 21)	-55.5566	D (83, 62, 63, 69)	162.284
R (50, 52)	1.3628	A (9, 14, 13)	113.0894	D (20, 6, 7, 22)	65.1420	D (61, 62, 71, 50)	-59.8183
R (50, 71)	1.4537	A (9, 14, 23)	107.8040	D (6, 7, 8, 9)	-178.8713	D (61, 62, 71, 72)	177.8849
R (52, 53)	1.2193	A (9, 14, 24)	107.8032	D (21, 7, 8, 9)	59.7055	D (61, 62, 71, 73)	60.3638
R (52, 54)	1.3622	A (13, 14, 23)	111.2475	D (22, 7, 8, 9)	-57.1086	D (63, 62, 71, 50)	-177.9587
R (54, 55)	1.4332	A (13, 14, 24)	111.1865	D (7, 8, 9, 10)	-0.0559	D (63, 62, 71, 72)	59.7445
R (55, 56)	1.0929	A (23, 14, 24)	105.3293	D (7, 8, 9, 14)	179.9718	D (63, 62, 71, 73)	-57.7766
R (55, 57)	1.0902	A (11, 31, 32)	125.5367	D (8, 9, 14, 13)	179.6639	D (83, 62, 71, 50)	60.8190
R (55, 58)	1.0929	A (11, 31, 33)	110.8549	D (8, 9, 14, 23)	56.2501	D (83, 62, 71, 72)	-61.4777
R (59, 60)	1.5383	A (32, 31, 33)	123.6084	D (8, 9, 14, 24)	-57.0007	D (83, 62, 71, 73)	-178.9989
R (59, 64)	1.5472	A (31, 33, 34)	115.9812	D (10, 9, 14, 13)	-0.3077	D (61, 62, 83, 84)	64.5722
R (59, 66)	1.0999	A (33, 34, 35)	108.8844	D (10, 9, 14, 23)	-123.7215	D (61, 62, 83, 85)	-175.614
R (59, 67)	1.0966	A (33, 34, 36)	108.9565	D (10, 9, 14, 24)	123.0277	D (61, 62, 83, 86)	-54.7535
R (60, 61)	1.5346	A (33, 34, 37)	107.6966	D (29, 11, 12, 13)	-58.7100	D (63, 62, 83, 84)	-171.8454
R (60, 82)	1.0929	A (35, 34, 36)	107.3084	D (29, 11, 12, 27)	63.8306	D (63, 62, 83, 85)	-52.0316
R (61, 62)	1.5473	A (35, 34, 37)	112.0762	D (29, 11, 12, 28)	178.7553	D (63, 62, 83, 86)	68.8289
R (61, 65)	1.0951	A (36, 34, 37)	111.8544	D (30, 11, 12, 13)	58.3637	D (71, 62, 83, 84)	-55.1394
R (61, 70)	1.0988	A (34, 37, 38)	109.5809	D (30, 11, 12, 27)	-179.0957	D (71, 62, 83, 85)	64.6744
R (62, 63)	1.5537	A (34, 37, 39)	109.0152	D (30, 11, 12, 28)	-64.1710	D (71, 62, 83, 86)	-174.4651
R (62, 71)	1.5557	A (34, 37, 40)	111.9541	D (31, 11, 12, 13)	179.7381	D (62, 63, 64, 59)	-46.7161
R (62, 83)	1.5422	A (38, 37, 39)	106.9408	D (31, 11, 12, 27)	-57.7213	D (62, 63, 64, 74)	-164.8352
R (63, 64)	1.554	A (38, 37, 40)	109.367	D (31, 11, 12, 28)	57.2034	D (62, 63, 64, 78)	76.7605
R (63, 68)	1.0987	A (39, 37, 40)	109.8532	D (12, 11, 31, 32)	-0.7811	D (68, 63, 64, 59)	-172.6433
R (63, 69)	1.0994	A (37, 40, 41)	109.9667	D (12, 11, 31, 33)	179.2714	D (68, 63, 64, 74)	69.2376
R (64, 74)	1.5426	A (37, 40, 42)	110.2915	D (29, 11, 31, 32)	-124.2391	D (68, 63, 64, 78)	-49.1667

Table A2. (cont.)

Definition	Value	Definition	Value	Definition	Value	Definition	Value
R (64, 78)	1.5442	A (37, 40, 43)	113.0554	D (29, 11, 31, 33)	55.8134	D (69, 63, 64, 59)	73.5383
R (71, 72)	1.0975	A (41, 40, 42)	106.8106	D (30, 11, 31, 32)	122.5221	D (69, 63, 64, 74)	-44.5808
R (71, 73)	1.0929	A (41, 40, 43)	108.2	D (30, 11, 31, 33)	-57.4255	D (69, 63, 64, 78)	-162.9850
R (74, 75)	1.0956	A (42, 40, 43)	108.2966	D (11, 12, 13, 14)	179.9954	D (59, 64, 74, 75)	-59.8695
R (74, 76)	1.0957	A (40, 43, 44)	109.4506	D (11, 12, 13, 25)	-58.1120	D (59, 64, 74, 76)	60.2475
R (74, 77)	1.0962	A (40, 43, 45)	109.6278	D (11, 12, 13, 26)	58.101	D (59, 64, 74, 77)	179.9017
R (78, 79)	1.0958	A (40, 43, 46)	108.155	D (27, 12, 13, 14)	58.0774	D (63, 64, 74, 75)	58.4273
R (78, 80)	1.0955	A (44, 43, 45)	107.3476	D (27, 12, 13, 25)	179.97	D (63, 64, 74, 76)	178.5443
R (78, 81)	1.0913	A (44, 43, 46)	111.1107	D (27, 12, 13, 26)	-63.817	D (63, 64, 74, 77)	-61.8015
R (83, 84)	1.0955	A (45, 43, 46)	111.1366	D (28, 12, 13, 14)	-58.1211	D (78, 64, 74, 75)	-179.6168
R (83, 85)	1.0963	A (43, 46, 47)	108.1938	D (28, 12, 13, 25)	63.7715	D (78, 64, 74, 76)	-59.4998
R (83, 86)	1.0908	A (2, 48, 49)	117.3421	D (28, 12, 13, 26)	179.9845	D (78, 64, 74, 77)	60.1545
		A (2, 48, 60)	122.6131	D (12, 13, 14, 9)	179.8187	D (59, 64, 78, 79)	175.3700
		A (49, 48, 60)	119.4724	D (12, 13, 14, 23)	-58.6882	D (59, 64, 78, 80)	-65.7201
		A (51, 50, 52)	116.973	D (12, 13, 14, 24)	58.3717	D (59, 64, 78, 81)	54.0926
		A (51, 50, 71)	120.4444	D (25, 13, 14, 9)	57.2888	D (63, 64, 78, 79)	52.7111
		A (52, 50, 71)	122.3007	D (25, 13, 14, 23)	178.7819	D (63, 64, 78, 80)	171.6211
		A (50, 52, 53)	125.9286	D (25, 13, 14, 24)	-64.1582	D (63, 64, 78, 81)	-68.5663
		A (50, 52, 54)	109.836	D (26, 13, 14, 9)	-57.6434	D (74, 64, 78, 79)	-66.0066
		A (53, 52, 54)	124.2354	D (26, 13, 14, 23)	63.8497	D (74, 64, 78, 80)	52.9034
		A (52, 54, 55)	114.5999	D (26, 13, 14, 24)	-179.0904	D (74, 64, 78, 81)	172.716
		A (54, 55, 56)	110.9065	D (11, 31, 33, 34)	179.7513		
		A (54, 55, 57)	105.5471	D (32, 31, 33, 34)	-0.1975		
		A (54, 55, 58)	110.8967	D (31, 33, 34, 35)	58.2614		
		A (56, 55, 57)	110.3643	D (31, 33, 34, 36)	-58.48		
		A (56, 55, 58)	108.748	D (31, 33, 34, 37)	-179.9964		
		A (57, 55, 58)	110.3634	D (33, 34, 37, 38)	58.7918		
		A (60, 59, 64)	113.5764	D (33, 34, 37, 39)	-57.9329		
		A (60, 59, 66)	107.9907	D (33, 34, 37, 40)	-179.6829		
		A (60, 59, 67)	109.2746	D (35, 34, 37, 38)	178.529		
		A (64, 59, 66)	109.0221	D (35, 34, 37, 39)	61.8043		
		A (64, 59, 67)	109.9415	D (35, 34, 37, 40)	-59.9457		
		A (66, 59, 67)	106.7958	D (36, 34, 37, 38)	-60.9018		
		A (48, 60, 59)	111.5607	D (36, 34, 37, 39)	-177.6265		
		A (48, 60, 61)	109.6038	D (36, 34, 37, 40)	60.6235		
		A (48, 60, 82)	104.959	D (34, 37, 40, 41)	-56.8683		
		A (59, 60, 61)	110.8291	D (34, 37, 40, 42)	60.6735		
		A (59, 60, 82)	109.4088	D (34, 37, 40, 43)	-177.9184		
		A (61, 60, 82)	110.3276	D (38, 37, 40, 41)	64.78		
		A (60, 61, 62)	113.3607	D (38, 37, 40, 42)	-177.6782		
		A (60, 61, 65)	109.4409	D (38, 37, 40, 43)	-56.2701		
		A (60, 61, 70)	108.6994	D (39, 37, 40, 41)	-178.136		
		A (62, 61, 65)	109.9555	D (39, 37, 40, 42)	-60.5942		
		A (62, 61, 70)	108.8351	D (39, 37, 40, 43)	60.8139		
		A (65, 61, 70)	106.296	D (37, 40, 43, 44)	-176.0216		
		A (61, 62, 63)	109.8025	D (37, 40, 43, 45)	-58.5269		
		A (61, 62, 71)	109.2595	D (37, 40, 43, 46)	62.7946		
		A (61, 62, 83)	110.7383	D (41, 40, 43, 44)	61.9328		
		A (63, 62, 71)	105.7773	D (41, 40, 43, 45)	179.4275		
		A (63, 62, 83)	112.8954	D (41, 40, 43, 46)	-59.251		
		A (71, 62, 83)	108.1865	D (42, 40, 43, 44)	-53.4944		
		A (62, 63, 64)	118.4261	D (42, 40, 43, 45)	64.0003		
		A (62, 63, 68)	109.3593	D (42, 40, 43, 46)	-174.6782		
		A (62, 63, 69)	106.8237	D (40, 43, 46, 47)	-176.01		
		A (64, 63, 68)	109.1325	D (44, 43, 46, 47)	63.8409		
		A (64, 63, 69)	106.5217	D (45, 43, 46, 47)	-55.6269		
		A (68, 63, 69)	105.8175	D (2, 48, 60, 59)	-94.6478		
		A (59, 64, 63)	109.1412	D (2, 48, 60, 61)	142.2188		
		A (59, 64, 74)	108.8645	D (2, 48, 60, 82)	23.7385		
		A (59, 64, 78)	110.6137	D (49, 48, 60, 59)	76.4415		
		A (63, 64, 74)	107.847	D (49, 48, 60, 61)	-46.6919		
		A (63, 64, 78)	112.9422	D (49, 48, 60, 82)	-165.1722		
		A (74, 64, 78)	107.3085	D (51, 50, 52, 53)	-177.4992		
		A (50, 71, 62)	115.5955	D (51, 50, 52, 54)	2.5225		
		A (50, 71, 72)	108.4042	D (71, 50, 52, 53)	-3.578		
		A (50, 71, 73)	106.476	D (71, 50, 52, 54)	176.4437		
		A (62, 71, 72)	108.9239	D (51, 50, 71, 62)	-83.4806		
		A (62, 71, 73)	109.4572	D (51, 50, 71, 72)	39.0924		
		A (72, 71, 73)	107.7046	D (51, 50, 71, 73)	154.7273		
		A (64, 74, 75)	111.4073	D (52, 50, 71, 62)	102.8041		
		A (64, 74, 76)	110.8894	D (52, 50, 71, 72)	-134.6229		
		A (64, 74, 77)	111.0838	D (52, 50, 71, 73)	-18.988		

Appendix 2

Table A3. Binding pockets parameters of the protease enzyme

Pocket ID	Volume/Å^3	Surface/Å^2	Depth/Å
P_0	1459.5100	2048.6700	30.0000
P_1	1381.7700	1631.5700	25.7400
P_2	784.1300	1110.4300	16.3900
P_3	741.8700	1096.8200	29.0800
P_4	610.4300	811.7500	24.8000
P_5	342.7500	402.4400	21.7900
P_6	273.2400	378.0600	12.3400
P_7	250.3300	382.1100	17.1200
P_8	241.4300	540.6000	16.0800
P_9	220.9700	450.4400	13.8500
P_10	216.1900	382.5000	11.5600
P_11	205.4000	404.2400	14.9200
P_12	186.6100	445.4700	10.6900
P_13	180.8300	440.2400	8.2300
P_14	179.8200	335.4300	14.2200
P_15	167.8100	165.7300	13.0700
P_16	153.2500	355.4100	8.9500
P_17	132.5600	138.1700	10.4800
P_18	129.2200	217.7700	7.1000
P_19	103.0900	226.2000	6.5400

Table A4. Binding tunnels parameters the protease enzyme

Tunnel ID	Bottleneck radius	Tunnel length	Tunnel curvature
t1	1.4370	2.8910	1.0310
t2	1.0960	11.0280	1.2920
t3	1.0960	32.8240	2.0190
t4	0.9580	36.8600	1.6850
t5	0.9070	49.2120	2.1500
t6	0.9040	52.6150	1.6710
t7	0.9070	62.6630	2.0830

Appendix 3

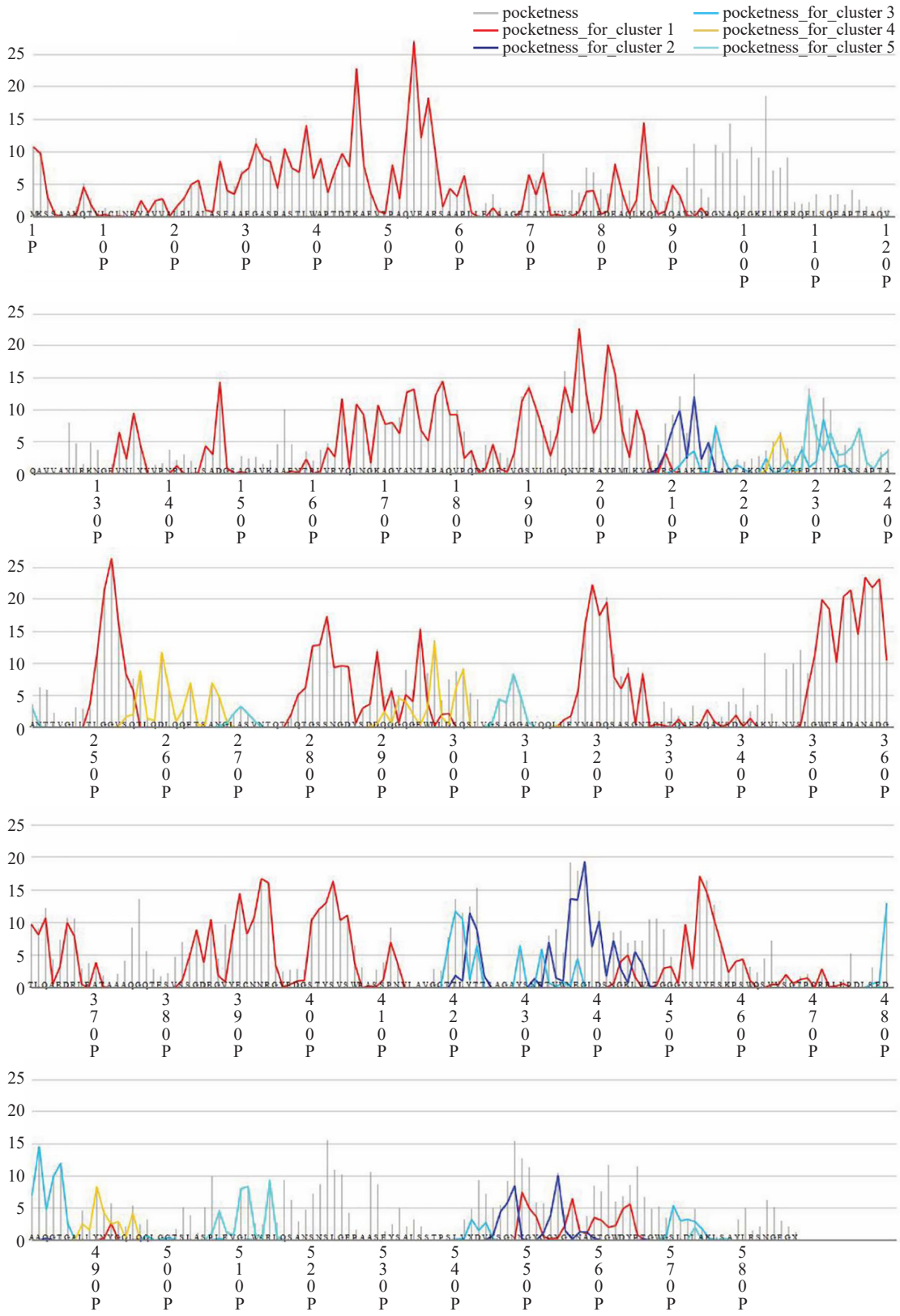

Figure A1. Graph of residue-based pocketness

Appendix 4

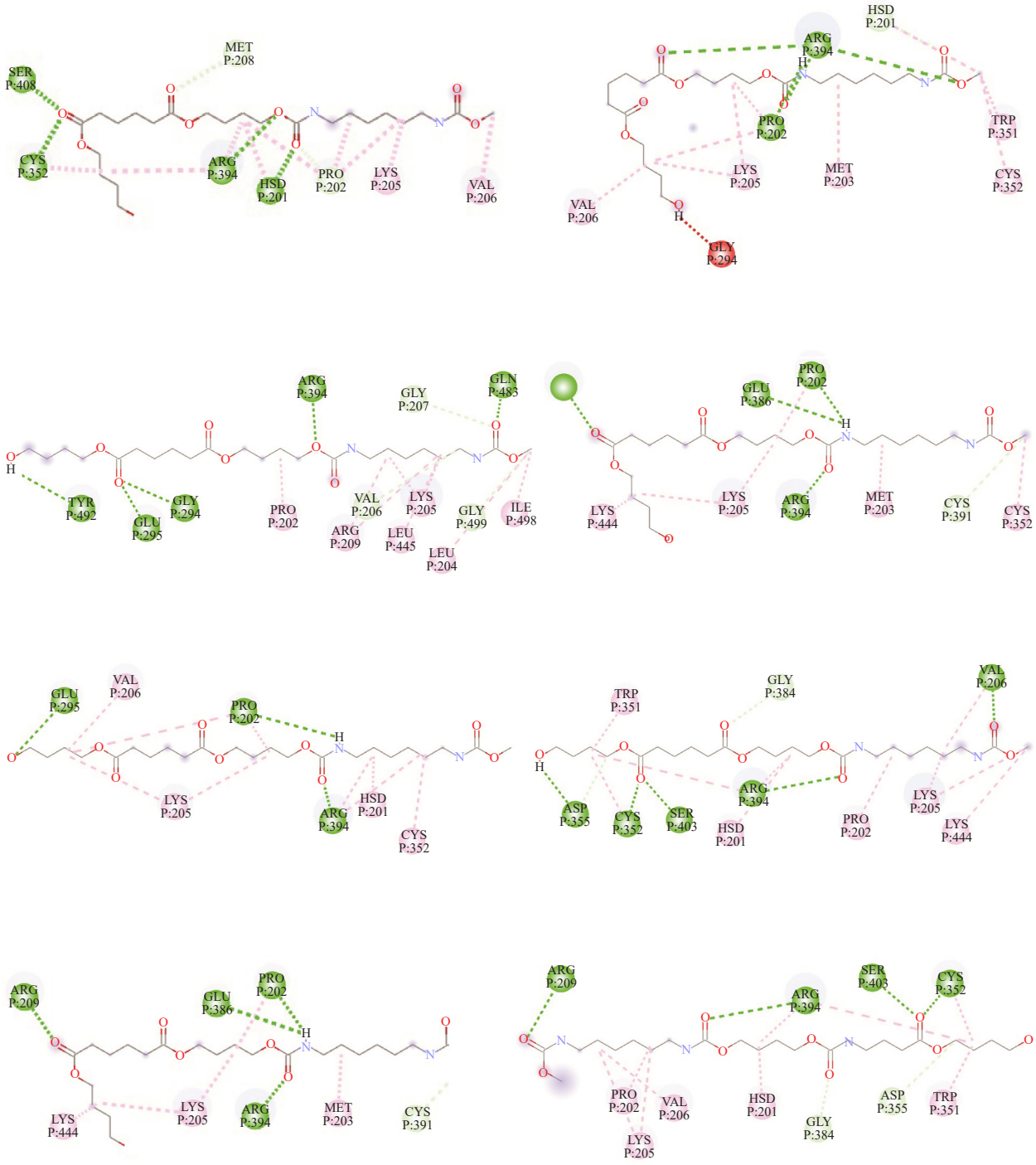
MET P:208
SER P:408
CYS P:352
ARG P:394
HSD P:201
PRO P:202
LYS P:205
VAL P:206
HSD P:201
ARG P:394
PRO P:202
TRP P:351
LYS P:205
MET P:203
CYS P:352
VAL P:206
GLY P:294
ARG P:394
GLY P:207
GLN P:485
TYR P:492
GLY P:294
GLU P:295
PRO P:202
VAL P:206
LYS P:205
ARG P:209
LEU P:445
GLY P:499
ILE P:498
LEU P:204
PRO P:202
GLU P:386
LYS P:444
LYS P:205
ARG P:394
MET P:203
CYS P:391
CYS P:352
GLU P:295
VAL P:206
PRO P:202
LYS P:205
ARG P:394
HSD P:201
CYS P:352
TRP P:351
GLY P:384
VAL P:206
ASP P:355
CYS P:352
SER P:403
ARG P:394
HSD P:201
PRO P:202
LYS P:205
LYS P:444
ARG P:209
GLU P:386
PRO P:202
LYS P:444
LYS P:205
ARG P:394
MET P:203
CYS P:391
ARG P:209
ARG P:394
SER P:405
CYS P:352
PRO P:202
VAL P:206
HSD P:201
GLY P:384
ASP P:355
TRP P:351
LYS P:205

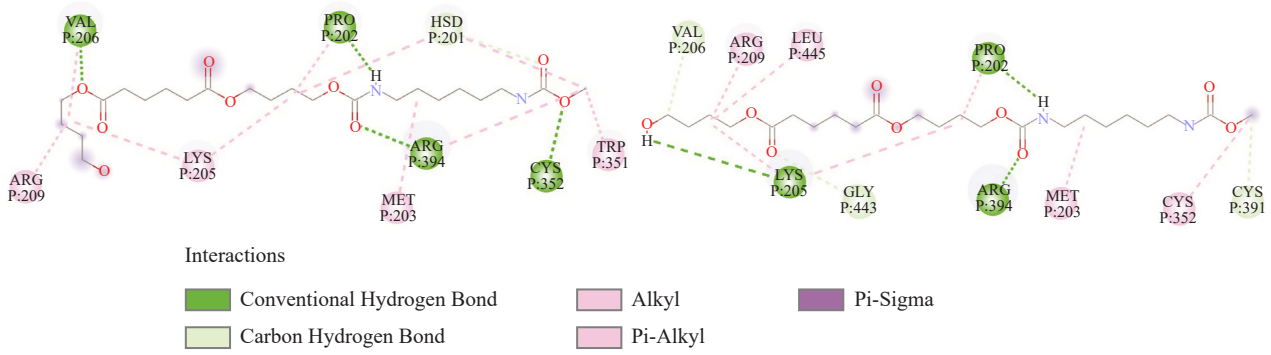

Figure A2. 2D interaction diagrams of ten Binding poses of PU-HDI with protease enzyme

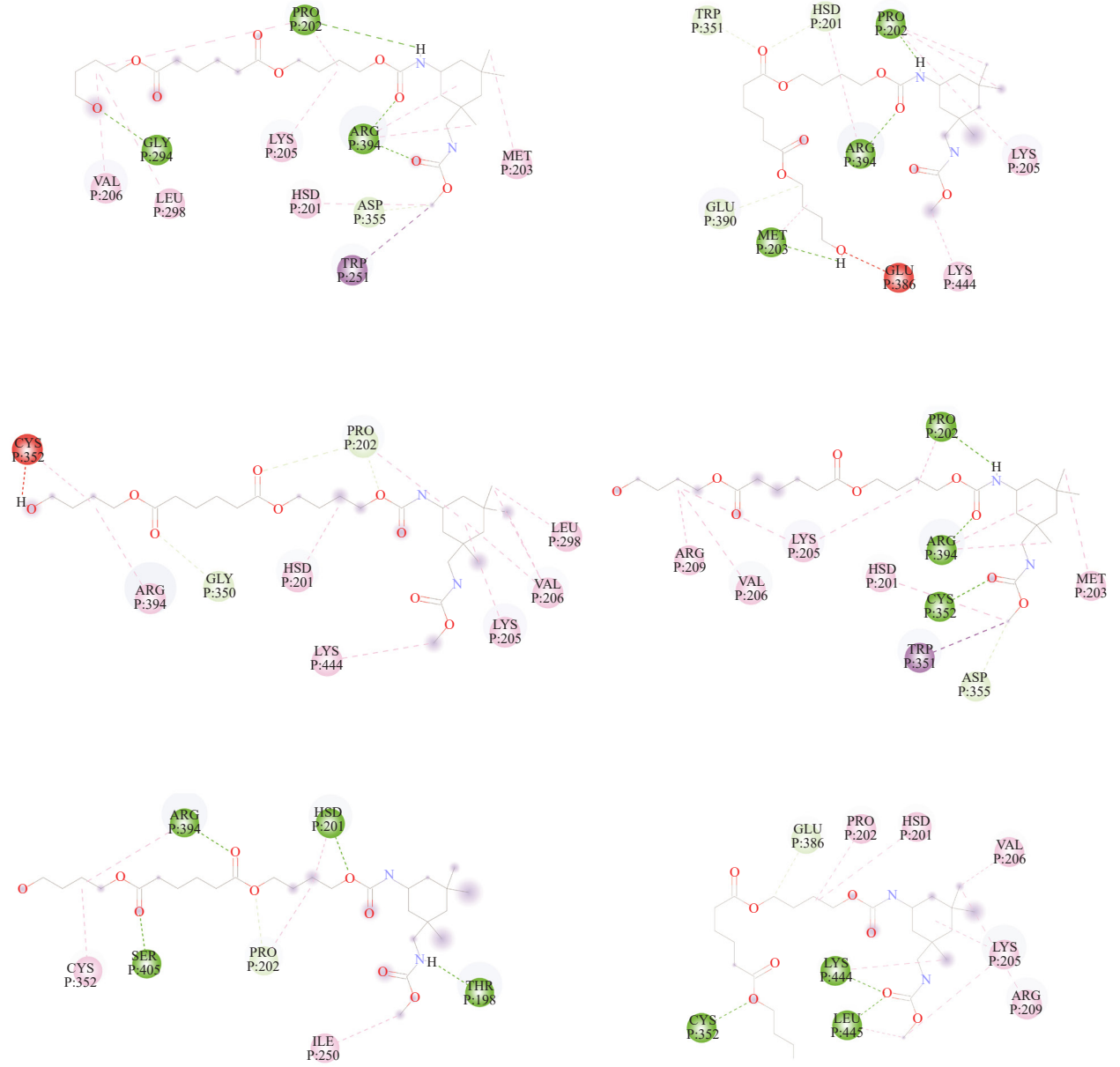

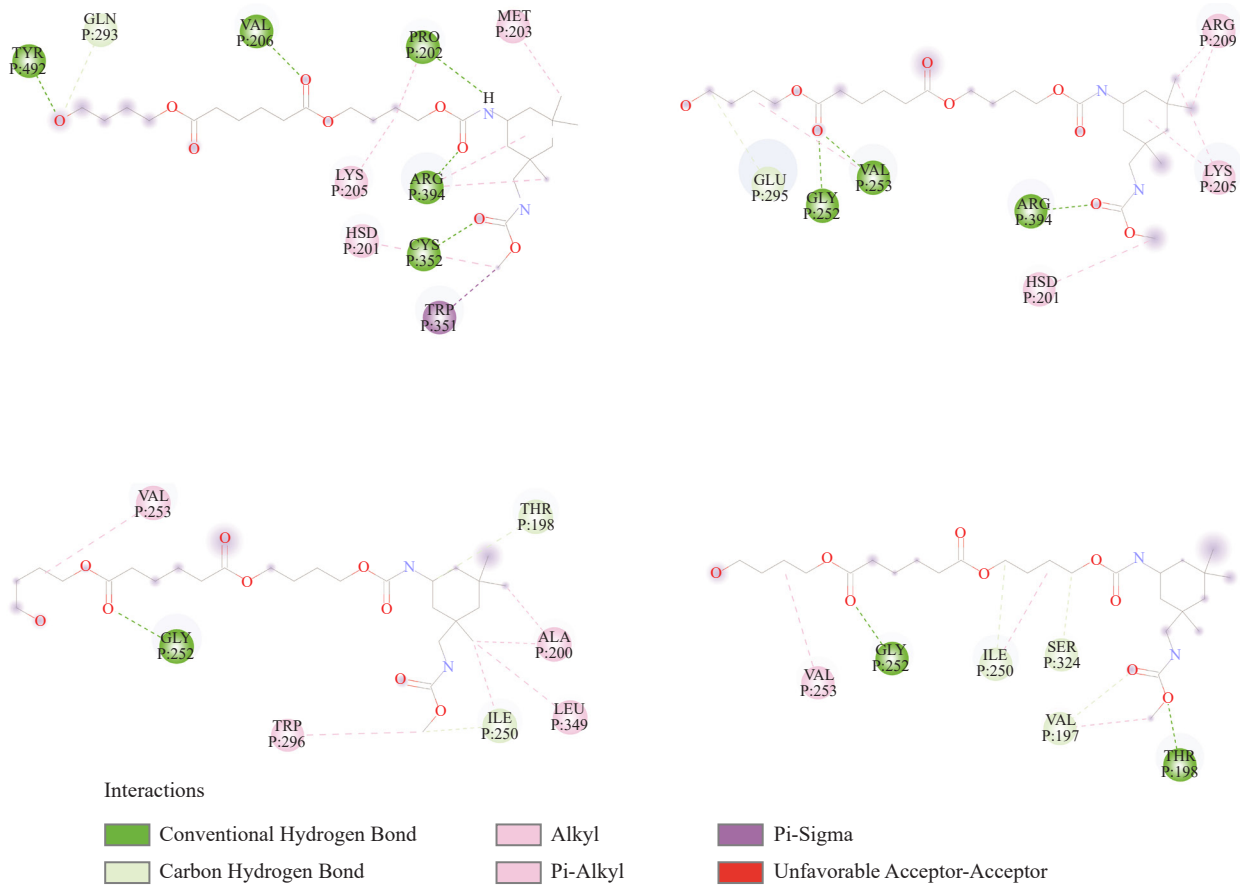

Figure A3. 2D interaction diagrams of ten Binding poses of PU-IPDI with protease enzyme

Appendix 5

Table A5. F- Fukui index, F+ Fukui index, F0 Fukui index and Dual-Descriptor values of PU-HDI

Atom number	F- Fukui index	F+ Fukui index	F0 Fukui index	Dual-Descriptor
1	0.0210	0.0057	0.0133	-0.0153
2	-0.0088	0.0282	0.0097	0.0194
3	0.0555	0.0156	0.0356	-0.0399
4	-0.0027	-0.0024	0.0026	-0.0004
5	-0.0027	-0.0024	0.0025	-0.0003
6	-0.0007	-0.0047	0.0027	0.0040
7	-0.0023	-0.0064	0.0044	0.0041
8	0.0097	0.0274	0.0185	0.0177
9	0.0042	0.1310	0.0676	0.1268
10	0.0461	0.0773	0.0617	0.0312
11	0.0046	-0.0170	0.0062	0.0124
12	-0.0034	-0.0081	0.0058	0.0047
13	-0.0026	-0.0080	0.0053	0.0054
14	0.0021	-0.0166	0.0073	0.0146
15	0.0143	0.0112	0.0127	-0.0031
16	0.0036	0.0036	0.0036	0.0000
17	0.0069	0.0061	0.0065	-0.0008
18	0.0084	-0.0013	0.0036	-0.0071
19	0.0018	0.0061	0.0039	0.0043
20	-0.0039	0.0116	0.0038	0.0077
21	0.0041	0.0128	0.0084	0.0088
22	0.0051	0.0126	0.0089	0.0075
23	0.0067	0.0368	0.0217	0.0301
24	0.0070	0.0396	0.0233	0.0326
25	0.0043	0.0099	0.0071	0.0057
26	0.0038	0.0097	0.0068	0.0059
27	0.0037	0.0097	0.0067	0.0060
28	0.0038	0.0098	0.0068	0.0060
29	0.0107	0.0375	0.0241	0.0268
30	0.0108	0.0391	0.0249	0.0283
31	0.0065	0.1331	0.0698	0.1266
32	0.0804	0.0776	0.0790	-0.0028
33	0.0212	0.0279	0.0246	0.0067
34	-0.0031	-0.0055	0.0043	0.0024
35	0.0062	0.0127	0.0094	0.0065
36	0.0060	0.0124	0.0092	0.0064
37	-0.0018	-0.0038	0.0028	0.0020
38	0.0034	0.0062	0.0048	0.0028
39	0.0059	0.0061	0.0060	0.0001
40	-0.0038	-0.0030	0.0034	-0.0008
41	0.0075	0.0045	0.0060	-0.0031
42	0.0091	0.0058	0.0075	-0.0033
43	-0.0086	-0.0002	0.0044	-0.0084
44	0.0263	0.0108	0.0185	-0.0155
45	0.0199	0.0052	0.0126	-0.0147

Table A5. (cont.)

Atom number	F- Fukui index	F+ Fukui index	F0 Fukui index	Dual-Descriptor
46	0.0723	-0.0015	0.0354	-0.0709
47	0.0129	0.0161	0.0145	0.0032
48	0.1117	0.0082	0.0599	-0.1035
49	0.0165	0.0087	0.0126	-0.0078
50	-0.0100	-0.0027	0.0063	-0.0074
51	0.0223	0.0103	0.0163	-0.0120
52	0.0142	0.0039	0.0091	-0.0103
53	0.0043	0.0004	0.0023	-0.0038
54	0.0127	0.0033	0.0080	-0.0094
55	0.0083	-0.0034	0.0025	-0.0049
56	0.0005	-0.0013	0.0004	0.0008
57	0.0088	0.0026	0.0057	-0.0062
58	0.0112	0.0058	0.0085	-0.0054
59	0.0008	-0.0002	0.0003	-0.0007
60	0.0106	0.0046	0.0076	-0.0060
61	0.0079	-0.0001	0.0039	-0.0077
62	0.0046	-0.0008	0.0019	-0.0038
63	0.0101	0.0015	0.0058	-0.0086
64	0.0144	0.0073	0.0109	-0.0071
65	-0.0112	-0.0026	0.0069	-0.0086
66	0.0235	0.0118	0.0176	-0.0118
67	0.0148	0.0034	0.0091	-0.0114
68	0.1265	0.0108	0.0686	-0.1157
69	0.0188	0.0171	0.0179	-0.0016
70	-0.0098	0.0664	0.0283	0.0567
71	0.0652	0.0324	0.0488	-0.0328
72	0.0225	0.0115	0.0170	-0.0111
73	-0.0051	-0.0047	0.0049	-0.0003
74	0.0092	0.0071	0.0081	-0.0021
75	0.0154	0.0117	0.0135	-0.0037
76	0.0103	0.0083	0.0093	-0.0019

Table A6. F- Fukui index, F+ Fukui index, F0 Fukui index and Dual-Descriptor values of PU-IPDI

Atom number	F- Fukui index	F+ Fukui index	F0 Fukui index	Dual-Descriptor
1	0.0232	0.0018	0.0125	-0.0214
2	-0.0101	0.0020	0.0041	-0.0081
3	0.0645	0.0043	0.0344	-0.0602
4	-0.0030	-0.0014	0.0022	-0.0017
5	-0.0029	-0.0020	0.0024	-0.0010
6	-0.0008	-0.0040	0.0024	0.0032
7	-0.0026	-0.0060	0.0043	0.0035
8	0.0084	0.0260	0.0172	0.0177
9	0.0040	0.1229	0.0634	0.1190
10	0.0451	0.0724	0.0588	0.0273
11	0.0044	-0.0164	0.0060	0.0120
12	-0.0033	-0.0077	0.0055	0.0044
13	-0.0026	-0.0076	0.0051	0.0050
14	0.0020	-0.0156	0.0068	0.0136
15	0.0149	0.0078	0.0114	-0.0071
16	0.0043	0.0030	0.0036	-0.0013
17	0.0072	0.0047	0.0059	-0.0026
18	0.0099	-0.0029	0.0035	-0.0071
19	0.0021	0.0058	0.0040	0.0037
20	-0.0046	0.0107	0.0030	0.0061
21	0.0057	0.0119	0.0088	0.0061
22	0.0052	0.0114	0.0083	0.0062
23	0.0066	0.0350	0.0208	0.0284
24	0.0062	0.0363	0.0212	0.0301
25	0.0042	0.0093	0.0067	0.0052
26	0.0043	0.0094	0.0068	0.0051
27	0.0037	0.0093	0.0065	0.0056
28	0.0035	0.0092	0.0063	0.0057
29	0.0108	0.0366	0.0237	0.0258
30	0.0106	0.0372	0.0239	0.0266
31	0.0065	0.1290	0.0677	0.1225
32	0.0790	0.0748	0.0769	-0.0043
33	0.0210	0.0271	0.0241	0.0061
34	-0.0030	-0.0053	0.0042	0.0023
35	0.0062	0.0121	0.0091	0.0059
36	0.0058	0.0118	0.0088	0.0060
37	-0.0018	-0.0037	0.0027	0.0018
38	0.0033	0.0059	0.0046	0.0026
39	0.0060	0.0058	0.0059	-0.0002
40	-0.0037	-0.0027	0.0032	-0.0011
41	0.0073	0.0040	0.0057	-0.0034
42	0.0091	0.0049	0.0070	-0.0042
43	-0.0086	-0.0008	0.0047	-0.0077
44	0.0260	0.0095	0.0178	-0.0165
45	0.0199	0.0041	0.0120	-0.0158

Table A6. (cont.)

Atom number	F- Fukui index	F+ Fukui index	F0 Fukui index	Dual-Descriptor
46	0.0716	-0.0020	0.0348	-0.0696
47	0.0128	0.0104	0.0116	-0.0024
48	0.1262	0.0007	0.0635	-0.1255
49	0.0165	0.0025	0.0095	-0.0140
50	0.0918	0.0086	0.0502	-0.0832
51	0.0157	0.0171	0.0164	0.0014
52	-0.0072	0.0668	0.0298	0.0596
53	0.0471	0.0349	0.0410	-0.0122
54	0.0179	0.0120	0.0149	-0.0059
55	-0.0042	-0.0048	0.0045	0.0006
56	0.0101	0.0105	0.0103	0.0005
57	0.0138	0.0124	0.0131	-0.0014
58	0.0050	0.0059	0.0054	0.0009
59	0.0048	-0.0005	0.0021	-0.0043
60	-0.0039	0.0001	0.0019	-0.0038
61	0.0005	-0.0011	0.0003	0.0006
62	0.0090	0.0007	0.0049	-0.0084
63	-0.0023	-0.0013	0.0018	-0.0010
64	0.0015	-0.0012	0.0001	-0.0003
65	0.0080	0.0031	0.0056	-0.0049
66	0.0112	0.0054	0.0083	-0.0059
67	0.0124	0.0043	0.0083	-0.0080
68	0.0141	0.0149	0.0145	0.0008
69	0.0076	0.0130	0.0103	0.0054
70	0.0088	0.0068	0.0078	-0.0021
71	-0.0071	-0.0028	0.0049	-0.0043
72	0.0291	0.0194	0.0242	-0.0096
73	0.0139	0.0088	0.0113	-0.0050
74	-0.0004	-0.0010	0.0007	0.0006
75	0.0065	0.0058	0.0061	-0.0007
76	0.0098	0.0041	0.0069	-0.0056
77	0.0143	0.0079	0.0111	-0.0064
78	-0.0042	-0.0015	0.0028	-0.0028
79	0.0124	0.0102	0.0113	-0.0022
80	0.0092	0.0076	0.0084	-0.0016
81	-0.0011	0.0026	0.0007	0.0015
82	0.0146	0.0036	0.0091	-0.0111
83	-0.0049	-0.0013	0.0031	-0.0036
84	0.0040	0.0123	0.0082	0.0083
85	0.0141	0.0157	0.0149	0.0016
86	0.0075	0.0099	0.0087	0.0023